國立臺灣大學工學院應用力學研究所

碩士論文

Institute of Applied Mechanics
College of Engineering
National Taiwan University
Master's Thesis

# 運用最佳控制理論及訓練表現模型設計運動員之最適訓練計畫

# Using Optimal Control Theory and Training-performance Model to Design Optimal Training Programs for Athletes

楊益

Yi Yang

指導教授：林哲宇 博士

Advisor: Che-Yu Lin, Ph.D.

中華民國 114 年 6 月

June, 2025

doi:10.6342/NTU202501357

# 誌謝

在求學過程中，首先感謝口試委員劉立偉與李宇修教授對本論文的指教，使本論文能夠更加完整，接著，我特別感謝指導教授林哲宇老師。在整個研究中，林老師給予我極大的協助與支持。每當我在研究上遇到瓶頸時，老師總能適時提供具體且有效的建議，使研究能夠順利推進。在撰寫學術期刊論文的過程中，無論是內容架構的調整，或是回應審稿意見的撰寫，老師都不吝給予指導，讓我學會了撰寫期刊文章與回覆評論的實務技巧，這對我幫助良多。在日常的相處中，我也深受老師治學態度的影響。尤其在論文後期，當我多次重複相同錯誤時，老師仍耐心細心地一一指正，讓我深刻感受到老師發自內心希望我能夠成長與進步的用心。

回顧這短短兩年的時間，我完成了碩士論文、投稿國際期刊、參與海報發表，甚至順利取得昆士蘭大學博士班的入學資格，這些成果的背後，都離不開林老師一路以來的指導與支持。期冀自己能帶著在老師身上學到的態度與精神，持續在未來的學術道路上努力前行。除了學術外，我要感謝台大橄欖球隊讓我在碩士期間得以繼續延續橄欖球員的生涯。縱使我只參與過一次大專盃比賽，但能與隊友們一起奪下亞軍獎盃，雖有些許遺憾，卻從不後悔，這段經歷將成為我難忘的回憶。特別感謝教練林威名，不僅在球技上提供指導，更在我擔任橄欖球裁判的道路上給予諸多協助。尤其是在去年舉薦我擔任 U19 橄欖球國際賽事的助理裁判，讓我有機會累積寶貴的國際賽經驗。

同時也感謝台灣橄欖球裁判聯盟的所有夥伴們，持續提供比賽場次與建議，讓我能在裁判的道路上不斷成長。衷心感謝正德國中教練劉曾祥、竹圍高中教練李建霖與台灣無惑俱樂部，經常性地提供我執法機會，不僅精進我執法技術，也使我在碩士期間可以無後顧之憂地學習與生活。

最後，我要感謝我的家人和女朋友子樂。你們一路以來的理解與支持，是你們讓我能無畏挑戰、安心追求學術與人生的理想。無論是情緒上的安慰、生活上的支援，還是默默的陪伴與鼓勵，都是我最堅強的後盾。我深知這段求學之路並不容易，若沒有你們的陪伴，我取得現在得成就。



doi:10.6342/NTU202501357

# 中文摘要

本研究提出一種新的方式，以最佳控制理論結合訓練-表現模型，設計個人化的最佳訓練計畫，目的在幫助運動員在競賽日達到最佳表現，同時預防過度訓練與使用傷害的可能。研究裡採用的訓練-表現模型為 Banister Impulse-Response model 的概念延伸，能夠描述訓練負荷（控制變數）、體能（正向影響）、疲勞（負向影響）與表現之間的動態關係。

研究所設計的目標函數，旨在透過提升體能與減少疲勞，以在比賽當日最大化表現，同時在整個訓練期間內盡量減少總訓練負荷。為求解此最佳控制問題，本研究透過前向-後向掃描法（Forward-Backward Sweep Method），已獲得訓練負荷、體能、疲勞與表現等變數隨時間之最佳變化。結果指出，與沒有最佳控制相比，以最佳控制理論可有效降低總訓練負荷並提升比賽日的表現。此外，透過起停式控制 (Bang-Bang control)，訓練負荷可在保持一段期間內恆定，僅於特定時間點進行切換，讓訓練計畫更符合實務操作，更提升效率與最終表現。

本研究奠定了結合訓練-表現模型與最佳控制理論在運動科學領域之基礎，證實其可行性與潛力。未來可導入更符合實際生理現象的非線性模型，以實驗驗證，來建立能真正協助運動員規劃訓練、提升表現並預防過度訓練的科學化系統。

**關鍵字**: 體適能疲勞模型、運動訓練和運動表現、電腦計算與數學模擬、運動科學、前向後向掃瞄法、起停式控制



doi:10.6342/NTU202501357

# ABSTRACT

To support athletes in reaching peak performance on competition day meanwhile reducing the risk of overtraining and overuse injuries, this study introduces a novel method that combines optimal control theory with a training-performance model to develop individualized, optimal training programs. The performance model utilized in this work is an extended version of the Banister Impulse-Response model, capturing the dynamic interactions between training load, fitness (representing positive adaptation), fatigue (representing negative effects), and overall performance.

The aim of the developed framework for optimal control is to maximize performance at the time of competition by increasing fitness and reducing fatigue, while concurrently minimizing the total training load throughout the training period. The Forward-Backward Sweep Method is employed to address the optimal control problem, yielding time-dependent trajectories of training load, fatigue, fitness, and performance. Simulation outcomes indicate that incorporating optimal control leads to improved competition-day performance with a lower cumulative training load compared to non-optimized approaches. Additionally, the implementation of bang-bang control strategies, where training loads are held constant over specific intervals, offers practical benefits, enhancing both training efficiency and final performance outcomes.

This study lays the foundation for applying optimal control theory in sports science, providing a systematic method for developing personalized training programs tailored to individual physiological characteristics. Future work should incorporate more physiologically realistic, nonlinear performance models and validate the proposed method with experimental data to advance toward practical and science-based training optimization for athletes.



doi:10.6342/NTU202501357

**KEYWORDS:** Fitness-Fatigue Model, athletic training and performance, computational and mathematical modeling, sports science, Forward-Backward Sweep Method, Bang-Bang Control

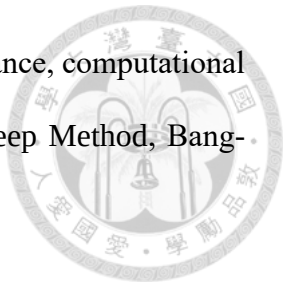



doi:10.6342/NTU202501357

# CONTENTS





doi:10.6342/NTU202501357

doi:10.6342/NTU202501357

# LIST OF FIGURES





doi:10.6342/NTU202501357

doi:10.6342/NTU202501357

doi:10.6342/NTU202501357

# LIST OF TABLES





doi:10.6342/NTU202501357

doi:10.6342/NTU202501357

# Chapter 1 Introduction

## 1.1 Background and Motivation

The principal focus of athletic training is to enhance athletes' performance during competitions [1]. Achieving this goal requires coaches and trainers to meticulously craft training regimens aligned with performance optimization. Nonetheless, implementing such targeted strategies in practice remains a complex task. In many instances, training programs are still predominantly shaped by individual experience, intuition, and a trial-and-error process, with limited integration of empirical data or systematic analysis [2,3].

In recent years, computational modeling and simulation have become valuable tools in the evaluation of athletic performance and injury prevention. These methods are increasingly adopted in sports science to provide detailed insights into the biomechanics of movement and muscle coordination. For example, Taylor et al. [4] employed an upper limb model to analyze muscle stress during a tennis serve, while Seth et al. [5] applied a unimanual musculoskeletal model to explore muscular contributions to shoulder and upper arm motion.

Despite their usefulness in exploring performance-related factors, such computational techniques are seldom used to directly guide decisions regarding training strategies—an essential part of athletic preparation. Planning training loads to achieve peak condition often continues to depend on subjective judgment and experience rather than on scientific optimization. This conventional methodology does not ensure that athletes will reach their peak fitness or perform optimally on competition day. Therefore, establishing a scientific framework for the systematic and optimal planning of training programs is crucial for maximizing athletic potential.



doi:10.6342/NTU202501357

To automate the simulation process in pursuit of optimal outcomes, optimal control theory (OCT) offers a compelling approach. As a robust mathematical framework, OCT facilitates the identification of input signals for dynamic systems that either maximize or minimize a defined performance objective [6–9]. Depending on whether the control function exhibits linear or higher-order characteristics, the resulting optimal solutions may be either continuous or piecewise, which corresponds well with common practices in training program development [10–12]. This study seeks to develop a practical methodology that combines OCT with performance modeling to systematically construct training plans, ensuring athletes can achieve peak condition precisely on the day of competition.

## 1.2 Literature Review

This section reviews relevant literature across two core domains: athletic training and OCT. The foundational concept of periodized training in sports was pioneered by Leo Pavlovic Matveyev [13], who is widely recognized as the father of modern training periodization. In his influential work *Fundamentals of Sports Training,* Matveyev proposed that when a competition is still some time away, athletes should begin with lower-intensity training or lighter resistance, gradually increasing the workload as the event approaches. Conversely, training volume should follow an inverse pattern—starting with the highest volume early in the program and tapering off as the competition nears. While coaches often rely on established guidelines to structure their athletes' training regimens, another critical aspect of training management lies in continuously assessing and understanding an athlete's performance level throughout the training process.



doi:10.6342/NTU202501357

Various methods have been developed by researchers to assess athletic performance. As early as 1923, Hill and Lupton proposed that an athlete's maximal oxygen uptake could serve as an upper boundary of their performance capacity [14]. Although this measurement has proven useful, it presents inherent risks—particularly for individuals with preexisting medical conditions such as cardiovascular disease. As a result, alternative, less invasive estimation techniques have been proposed [15–19]. Nevertheless, this approach is not without its shortcomings. For instance, athletes with comparable maximal oxygen uptake values may exhibit significant differences in endurance. Moreover, the testing procedure typically requires subjects to exert themselves to their physical limits, which increases the risk of injury.

To overcome these issues, particularly in predicting individual performance trajectories, the Fitness-Fatigue Model (FFM) has gained recognition as a practical tool for guiding long-term training strategies [3,20–25]. The FFM describes how accumulated training loads influence athletic performance. Its simplicity—focusing exclusively on the relationship between training input and performance output—makes it especially suitable for forecasting performance on specific target dates, such as competition day. Additionally, the use of arbitrary impulse units allows the model to be adapted to various input formats, including metrics like heart rate and power output, providing coaches with considerable flexibility. The increasing availability of real-time monitoring technologies and software platforms has further enhanced the model's utility and accessibility [3].

Despite its popularity, the FFM has been subject to significant scrutiny over the decades [26–29]. For example, Hellard et al. [26] pointed out that the high correlation between fitness and fatigue parameters often results in poor model conditioning. In response, researchers have proposed several refinements to improve its predictive accuracy. Turner et al. [29] introduced nonlinear dynamics into the original framework



doi:10.6342/NTU202501357

to account for phenomena such as overtraining and saturation effects, while Peng et al. [30] employed Bayesian inference techniques to enhance the model's fitting capabilities. Although there is still room for improvement, the model remains widely used by practitioners. For instance, Luteberget et al. [31] reported its application in football clubs for data analysis, while Lamberti et al. [32] utilized the FFM to evaluate outcomes of pain-free exercise programs.

Recent studies have further broadened the model's application across diverse sporting contexts. Mandorino et al. [33], for example, integrated the Banister model with machine learning algorithms to develop a novel performance index, examining its correlation with physical and tactical variables in elite football. Jeffries et al. [34] proposed incorporating the FFM within a broader conceptual framework to inform the development and validation of athlete monitoring tools. In another case, Borrani et al. [35] applied the FFM alongside complementary analytical methods to assess performance and training load adaptation in elite short-track speed skaters. These advancements reflect the model's continued evolution through interdisciplinary research and methodological innovation. Nonetheless, despite these promising developments, there is still a notable gap in the literature regarding the use of the FFM for systematically designing training programs aimed at achieving clearly defined performance targets.

To bridge the existing gap, OCT presents a promising avenue. As a mathematical framework, OCT is designed to determine the best possible control input applied to a dynamic system in order to optimize a specified performance criterion. These systems—whether governed by discrete, ordinary, or partial differential equations—feature variables that can be influenced through external control mechanisms [6–9].

OCT has been successfully applied across various disciplines. In aerospace engineering, for example, a dynamic system may represent a spacecraft, with control



doi:10.6342/NTU202501357

inputs corresponding to thruster activity, and the objective being to reach the Moon while minimizing fuel usage [36]. In the field of economics, OCT can model a national economy, using policy instruments to reduce unemployment [37]. In biomedical applications, it has been used to optimize drug administration schedules, aiding in the design of chemotherapy protocols for conditions such as HIV [38]. These examples underscore OCT's strength in manipulating controllable variables to achieve clearly defined goals across diverse contexts.

When viewed through the lens of integrating sports science with OCT, it becomes apparent that existing efforts to refine the FFM have largely centered on improving data fitting techniques [29, 30, 39], rather than leveraging the model for optimizing the structure of training itself. To address this limitation and enhance the strategic design of training programs, the present study employs OCT to determine the most effective training load. The aim is to ensure that athletes attain their peak physical condition precisely on the day of competition, through a systematic and quantitatively informed approach.

## 1.3 The Purposes of the Present Study

The central aim of this research is to develop a computational approach that integrates OCT with models of athletic performance to develop personalized exercise regimens. In contrast to traditional practices—which often rely on heuristic rules or coaches' intuition—this method offers a systematic and objective way to structure training based on clearly defined performance targets. By applying optimal control techniques, it becomes possible to determine how training loads should vary over time to help athletes



doi:10.6342/NTU202501357

reach peak condition on the day of competition, while also improving efficiency and reducing the risk of overtraining.

The study is guided by the following objectives:

1. To investigate how optimal control and performance modeling can be jointly applied to create effective training strategies.
2. To illustrate how this approach can be personalized by adjusting key parameters according to physiological characteristics or performance data.
3. To examine methods for modifying and refining training schemes, thereby enhancing their practicality and relevance in real-world settings.

Through this strategy, the study aims to offer a flexible and evidence-based tool for coaches and sports scientists. The anticipated contribution spans both theoretical advancements in control applications and practical improvements in optimizing athletic training outcomes.



doi:10.6342/NTU202501357

# Chapter 2 Optimal Control Theory

The introduction to OCT in current chapter is organized and explained building upon the work of Lenhart and Workman [38].

## 2.1 The Fundamental Problem and Necessary Conditions

### 2.1.1 Definition

OCT offers a powerful mathematical foundation for decision-making in fields such as engineering, economics, and biomedical science. When applied to a specific dynamic system with defined performance criteria, OCT enables the systematic identification of control inputs that guide the system toward the most favorable outcome. In a standard setting involving ordinary differential equations, the problem includes a control input and a state variable. The state dynamics are described by a differential equation, where the control function plays a direct role in shaping system behavior.

$$x'(t) = g\big(t, x(t), u(t)\big). \tag{2.1.1}$$

By modifying the input function $u(t)$, the evolution of the state variable $x(t)$ s consequently affected. Thus, the relationship between the input and the system's state can be viewed as a mapping from $u(t)$ to the resulting state $x = x(u)$. The core problem involves identifying a piecewise continuous input $u(t)$ and the corresponding state trajectory $x(t)$ that together maximize a given performance measure, often expressed as a functional.



doi:10.6342/NTU202501357

$$\begin{aligned} \max_{u} \quad & \int_{t_0}^{t_1} f\big(t, x(t), u(t)\big)dt \\ subject\ to \quad & x'(t) = g\big(t, x(t), u(t)\big) \\ & x(t_0) = x_0,\ \ x(t_1)\ free. \end{aligned} \tag{2.1.2}$$

The input that yields the best performance according to the chosen criterion is referred to as the optimal input. When the state value at time $t_1$, $x(t_1)$ is free, it means there is no restriction on its value. Typically, the problem is formulated over a continuous time interval. Consequently, the functions involved—often denoted as $f$ and $g$—are assumed to be smoothly varying in terms of their arguments. As a result, the control inputs change without abrupt jumps except at certain points, and the corresponding state variables evolve in a manner that is differentiable except possibly at a limited number of instances.

### 2.1.2 Objective Functional

To formulate an OCP, one must specify both the system's governing equation and a functional expressing the intended objective. This functional involves both the state and control variables to develop a strategy that guides the system toward the desired performance. The OF is generally can be written as:

$$J(u) = \int_{t_0}^{t_1} f\big(t, x(t), u(t)\big)dt. \tag{2.1.3}$$

The formulation of the OF varies according to the specific problem and objectives set by the decision-maker. In OCPs, the control function is adjusted to optimize the OF, ultimately achieving a predefined goal. For instance, one might regulate the concentration of chemical nutrients to both maximize bacterial growth and minimize resource consumption.



doi:10.6342/NTU202501357

When defining the OF, it is important to account for the problem's constraints and the desired system performance criteria. These constraints may include, but are not limited to, biological growth rates, reaction speeds, environmental conditions, and financial costs. The OF can be formulated as a single function or as a combination of multiple objectives to satisfy the decision-maker's goals. In this study, we refer to a previously established example and present the formulation of the OCP accordingly [38]

$$\begin{aligned} &\max_{u} \quad Cx(1) - \int_0^1 p(t)^2 dt \\ &subject\ to \quad x'(t) = rx(t) + Mp(t)x(t) - Np(t)^2 e^{-x(t)} \\ &\qquad x(0) = x_0, \ \ M, N, C \geq 0. \end{aligned} \tag{2.1.4}$$

In this context, $p(t)$ denotes the amount of chemical introduced at time $t$, while $x(t)$ represents the bacterial concentration at the same moment. The parameter $M$ reflects the relative efficacy of the chemical nutrient in stimulating growth, and $N$ captures the influence exerted by the byproduct. By varying these parameters, decision-makers can gain deeper insights into their respective effects on the system's behavior.

In many OCPs, the control input within the OF is commonly modeled as either a linear (first-order) or quadratic (second-order) function. These particular forms are favored because they guarantee a unique solution, facilitate efficient computation, and correspond well with practical physical interpretations [38].

### 2.1.3 Necessary Conditions

A fundamental approach to solving OCPs is to establish necessary conditions that the optimal input and its associated state must satisfy. This approach, pioneered by Pontryagin and his collaborators in the 1950s [38], introduces auxiliary variables—known as adjoint functions—that incorporate the system's dynamic constraints into the



doi:10.6342/NTU202501357

performance criterion. This idea is similar to the role of Lagrange multipliers in constrained optimization, where these auxiliary functions enforce the problem's restrictions throughout the solution process. The method proceeds by first specifying the conditions the adjoint variables must meet, and then expressing the optimal input as a function of the optimal state and the corresponding adjoint variables via differentiation.

Assuming the existence of an optimal control $u^*$ that varies smoothly except possibly at a finite number of points, together with its corresponding state $x^*$, it follows that for any admissible control $u$, the performance measure satisfies $J(u) \leq J(u^*) < \infty$. Let $h(t)$ denote a variation function with similar smoothness properties, and $\epsilon \in \mathbb{R}$ be a constant. Then,

$$u^{\epsilon}(t) = u^*(t) + \epsilon h(t) \tag{2.1.5}$$

denotes an alternative control function that changes smoothly except possibly at a limited number of points.

Let $x^{\epsilon}$ denote the state trajectory corresponding to the control $u^{\epsilon}$, namely, which satisfies the differential equation

$$\frac{d}{dt}x^{\epsilon}(t) = g\big(t, x^{\epsilon}(t), u^{\epsilon}(t)\big) \tag{2.1.6}$$

at points where $u^{\epsilon}$ is continuous. Since all trajectories originate from the same initial condition, we set $x^{\epsilon}(t_0) = x_0$ as illustrated in Figure 2-1.



doi:10.6342/NTU202501357

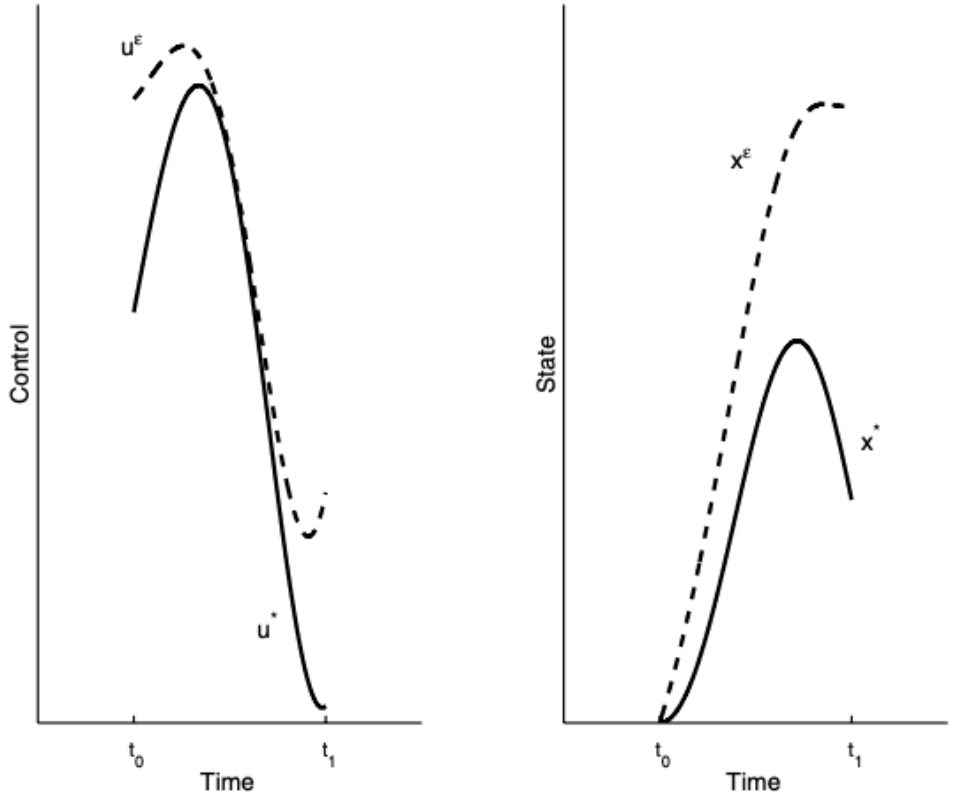


Figure 2-1 The optimal control $u^*$ and state $x^*$ (shown in solid lines) are plotted alongside $u^\epsilon$and $x^\epsilon$ (depicted with dashed lines) [38].

It is straightforward to see that $u^\epsilon(t)$ approaches $u^*(t)$ for every $t$ as $\epsilon$ tends to zero. Furthermore, the partial derivative of $u^\epsilon(t)$ in terms of $\epsilon$ evaluated at $\epsilon = 0$ equals $h(t)$:

$$\left.\frac{\partial u^\epsilon(t)}{\partial \epsilon}\right|_{\epsilon=0} = h(t). \tag{2.1.7}$$

A similar property applies to the state $x^\epsilon$. Under the given assumptions on the function $g$, it follows that

$$x^\epsilon(t) \to x^*(t) \tag{2.18}$$

for each fixed $t$. Moreover, the derivative



doi:10.6342/NTU202501357

$$\left.\frac{\partial x^{\epsilon}(t)}{\partial \epsilon}\right|_{\epsilon=0} \tag{2.1.9}$$

exists for all $t$. While the explicit value of this derivative is not critical here, its existence is essential for the analysis.

The OF evaluated at $u^{\epsilon}(t)$ is given by

$$J(u^{\epsilon}) = \int_{t_0}^{t_1} f\big(t, x^{\epsilon}(t), u^{\epsilon}(t)\big)dt, \tag{2.1.10}$$

where $\lambda(t)$ represents the adjoint function. This function is assumed to be differentiable almost everywhere on the interval $[t_0, t_1]$, with its specific form to be determined. By applying the Fundamental Theorem of Calculus, we obtain

$$\int_{t_0}^{t_1} \frac{d}{dt}[\lambda(t)x^{\epsilon}(t)]\,dt = \lambda(t_1)x^{\epsilon}(t_1) - \lambda(t_0)x^{\epsilon}(t_0). \tag{2.1.11}$$

Our expression for $J(u^{\epsilon})$ is represented by

$$J(u^{\epsilon}) = \int_{t_0}^{t_1} \frac{d}{dt}[\lambda(t)x^{\epsilon}(t)]\,dt + \lambda(t_0)x^{\epsilon}(t_0) - \lambda(t_1)x^{\epsilon}(t_1) =$$

$$\int_{t_0}^{t_1} \frac{d}{dt}\big[f\big(t, x^{\epsilon}(t), u^{\epsilon}(t)\big) + \lambda'(t)x^{\epsilon}(t) + \lambda(t)g\big(t, x^{\epsilon}(t), u^{\epsilon}(t)\big)\big]\,dt + \tag{2.1.12}$$

$$\lambda(t_0)x^{\epsilon}(t_0) - \lambda(t_1)x^{\epsilon}(t_1),$$

where $g\big(t, x^{\epsilon}(t), u^{\epsilon}(t)\big)$ denotes the derivative of $x^{\epsilon}(t)$ in terms of $t$ at several specific points. Since the maximum of $J$ in terms of the control $u$ is achieved at $u^{*}$, the derivative of $J(u^{\epsilon})$ in terms of $\epsilon$ evaluated at zero must vanish, i.e.,

$$0 = \frac{d}{d\epsilon}J(u^{\epsilon})\Big|_{\epsilon=0} = \lim_{\epsilon\to 0}\frac{J(u^{\epsilon}) - J(u^{*})}{\epsilon}. \tag{2.1.13}$$

This result enables the evaluation of the limit inside the integral. By applying a version of the Lebesgue Dominated Convergence Theorem [40–42], it is justified to interchange the limit and the integration operations, allowing differentiation to be performed under the integral sign. This reasoning relies on the integration domain being compact and the integrand exhibiting smooth behavior except at a finite number of



doi:10.6342/NTU202501357

points. Therefore,

$$0 = \frac{d}{d\epsilon} J(u^{\epsilon})\Big|_{\epsilon=0}$$

$$= \int_{t_0}^{t_1} \frac{\partial}{\partial \epsilon} \big[ f\big(t, x^{\epsilon}(t), u^{\epsilon}(t)\big) + \lambda'(t) x^{\epsilon}(t) \tag{2.1.14}$$

$$+ \lambda(t) g\big(t, x^{\epsilon}(t), u^{\epsilon}(t)\big) \big]\, dt \Big|_{\epsilon=0} - \frac{\partial}{\partial \epsilon} \lambda(t_1) x^{\epsilon}(t_1)\Big|_{\epsilon=0}.$$

Using chain rule to $f$ and $g$, we obtain

$$0 = \int_{t_0}^{t_1} \Big[ f_x \frac{\partial x^{\epsilon}}{\partial \epsilon} + f_u \frac{\partial u^{\epsilon}}{\partial \epsilon} + \lambda'(t) \frac{\partial x^{\epsilon}}{\partial \epsilon} + \lambda(t) \Big( g_x \frac{\partial x^{\epsilon}}{\partial \epsilon} + g_u \frac{\partial u^{\epsilon}}{\partial \epsilon} \Big) \Big]\, dt \Big|_{\epsilon=0} - \lambda(t_1) \frac{\partial x^{\epsilon}}{\partial \epsilon}\Big|_{\epsilon=0}. \tag{2.1.15}$$

Here, the terms $f_x$, $f_u$, $g_x$ and $g_u$ are evaluated at the point $\big(t, x^*(t), u^*(t)\big)$. By reorganizing the expressions in equation (2.1.15), we obtain

$$0 = \int_{t_0}^{t_1} \Big[ \frac{(f_x + \lambda(t) g_x + \lambda'(t))(\partial x^{\epsilon})}{\partial \epsilon(t)} \Big|_{\epsilon=0} + (f_u + \lambda(t)) h(t) \Big]\, dt - \lambda(t_1) \frac{\partial x^{\epsilon}}{\partial \epsilon}(t_1)\Big|_{\epsilon=0}. \tag{2.1.16}$$

To simplify Eq. (2.1.16), the adjoint function is chosen such that the coefficient multiplying

$$\frac{\partial x^{\epsilon}}{\partial \epsilon}(t)\Big|_{\epsilon=0} \tag{2.1.17}$$

vanishes. This leads to the requirement that the adjoint variable $\lambda(t)$ satisfies the differential equation

$$\lambda'(t) = -\big[ f_x\big(t, x^*(t), u^*(t)\big) + \lambda(t) g_x\big(t, x^*(t), u^*(t)\big) \big], \tag{2.1.18}$$

subject to the boundary condition

$$\lambda'(t_1) = 0. \tag{2.1.19}$$

Eq. (2.1.18) is referred to as the adjoint equation, while Eq. (2.1.19) is known as the



doi:10.6342/NTU202501357

transversality condition. With these, Eq. (2.1.16) can be simplified to

$$0 = \int_{t_0}^{t_1} \left[ f_u\left(t, x^*(t), u^*(t)\right) + \lambda(t) g_u\left(t, x^*(t), u^*(t)\right) \right] h(t) dt, \tag{2.1.20}$$

where $h(t)$ is an admissible variation function. Because this holds for all sufficiently regular $h(t)$, it follows that

$$f_u\left(t, x^*(t), u^*(t)\right) + \lambda(t) g_u\left(t, x^*(t), u^*(t)\right) = 0, \tag{2.1.21}$$

for every $t \in [t_0,\ t_1]$. This leads to the optimality condition expressed as

$$0 = \int_{t_0}^{t_1} \left[ f_u\left(t, x^*(t), u^*(t)\right) + \lambda(t) g_u\left(t, x^*(t), u^*(t)\right) \right]^2 dt, \tag{2.1.22}$$

which enforces

$$f_u\left(t, x^*(t), u^*(t)\right) + \lambda(t) g_u\left(t, x^*(t), u^*(t)\right) = 0. \tag{2.1.23}$$

These equations characterize the necessary conditions for optimal control and its associated state trajectory. In practice, rather than deriving these conditions from first principles for each new problem, they can be systematically obtained by introducing the Hamiltonian function $\mathcal{H}$, defined as

$$\mathcal{H}(t, x, u, \lambda) = f(t, x, u) + \lambda g(t, x, u), \tag{2.1.24}$$

which combines the integrand and the adjoint variable multiplied by the system dynamics.

The maximization of $\mathcal{H}$ in terms of $u$ at optimal control $u^*$ allows these conditions to be restated as

$$\frac{\partial \mathcal{H}}{\partial u} = 0 \ at \ u^* \rightarrow \ f_u + \lambda g_u = 0, \tag{2.1.25}$$

$$\lambda' = -\frac{\partial \mathcal{H}}{\partial x} \rightarrow \ \lambda' = -(f_x + \lambda g_x), \tag{2.1.26}$$

$$\lambda'(t_1) = 0, \tag{2.1.27}$$

Eq. (2.1.24) is referred to as the optimality condition, while Eq. (2.1.26) is known as the adjoint equation. Together with the state equation, which describes the system



doi:10.6342/NTU202501357

dynamics, these form the set of necessary conditions for solving the OCP. The state equation is given by:

$$x' = g(t, x, u) = \frac{\partial \mathcal{H}}{\partial \lambda}, x(t_0) = x_0. \tag{2.1.28}$$

## 2.2 Pontryagin's Maximum Principle

To solve the OCP, we utilize the necessary conditions previously established. In addition, two theorems are introduced to extend Pontryagin's Maximum Principle (PMP), providing a systematic approach for characterizing the optimal control solution [43].

**THEOREM 2.1**

*If* $u^*(t)$ *and* $x^*(t)$ *are optimal for Eq. (2.1.2), then there exists an adjoint variable* $\lambda(t)$, *which is differentiable except possibly at several specific points, such that the following inequality holds:*

$$\mathcal{H}\big(t, x^*(t), u(t), \lambda(t)\big) \leq \mathcal{H}\big(t, x^*(t), u^*(t), \lambda(t)\big), \tag{2.2.1}$$

for all admissible controls $u$ *at time* $t$, *where the Hamiltonian* $\hbar$ *is defined by*

$$\mathcal{H} = f\big(t, x(t), u(t), \lambda(t)\big) + \lambda(t) g\big(t, x(t), u(t)\big). \tag{2.2.2}$$

*In addition, the adjoint variable must satisfy the differential condition*

$$\lambda'(t) = -\frac{\partial \mathcal{H}\big(t, x^*(t), u^*(t), \lambda(t)\big)}{\partial x}, \tag{2.2.3}$$

$$\lambda(t_1) = 0. \tag{2.2.4}$$

Section 2.1.3 has presented the proof of this theorem. These conditions offer a structured approach to analyzing and solving OCPs, eliminating the need for explicit variation of the OF. By constructing the Hamiltonian and solving the corresponding



doi:10.6342/NTU202501357

state and adjoint equations, the optimal control strategy can be systematically obtained.

**THEOREM 2.2**

*Assume that both* $g(t,x,u)$ *and* $f(t,x,u)$ *are continuously differentiable with respect to all their arguments and are concave in terms of the control variable* $u$. *Let* $u^*$ *denote the optimal control associated with Eq. (2.1.2),* $x^*$ *its corresponding state, and* $\lambda(t)$ *an auxiliary function that is differentiable except at most at finitely many points, with* $\lambda(t) \geq 0$ *for all* $t$. *Suppose further that the condition*

$$0 = \mathcal{H}_u\big(t, x^*(t), u^*(t), \lambda(t)\big) \tag{2.2.5}$$

*is satisfied. Then for any admissible control* $u(t)$, *the following inequality holds:*

$$\mathcal{H}\big(t, x^*(t), u(t), \lambda(t)\big) \leq \mathcal{H}\big(t, x^*(t), u^*(t), \lambda(t)\big). \tag{2.2.6}$$

**PROOF** Fix an arbitrary time point $t_0 \leq t \leq t_1$ and consider a control value $u(t)$. Then, we compute

$$\begin{aligned}
&\mathcal{H}\big(t, x^*(t), u^*(t), \lambda(t)\big) - \mathcal{H}\big(t, x^*(t), u(t), \lambda(t)\big) \\
&= \big[f\big(t, x^*(t), u^*(t), \lambda(t)\big) + \lambda(t) g\big(t, x^*(t), u^*(t)\big)\big] \\
&- \big[f\big(t, x^*(t), u(t), \lambda(t)\big) + \lambda(t) g\big(t, x^*(t), u(t)\big)\big] \\
&= \big[f\big(t, x^*(t), u^*(t), \lambda(t)\big) - f\big(t, x^*(t), u(t), \lambda(t)\big)\big] \\
&+ \lambda(t)\big[g\big(t, x^*(t), u^*(t)\big) - g\big(t, x^*(t), u(t)\big)\big] \\
&\geq \big(u^*(t) - u(t)\big) f_u\big(t, x^*(t), u^*(t)\big) \\
&+ \lambda(t)\big(u^*(t) - u(t)\big) g_u\big(t, x^*(t), u^*(t)\big) \\
&= \big(u^*(t) - u(t)\big)\, \mathcal{H}_u\big(t, x^*(t), u^*(t), \lambda(t)\big) = 0.
\end{aligned} \tag{2.2.7}$$



doi:10.6342/NTU202501357

The inequality above results from the application of the tangent line property (first-order condition) due to the concavity of $f$ and $g$ in terms of $u$, and the assumption that $\lambda(t) \geq 0$.

A similar reasoning applies to minimization problems. If the objective is to minimize the functional, and both $f$ and $g$ are convex in $u$, the Hamiltonian will instead satisfy the reversed inequality:

$$\mathcal{H}\big(t, x^*(t), u(t), \lambda(t)\big) \geq \mathcal{H}\big(t, x^*(t), u^*(t), \lambda(t)\big), \tag{2.2.8}$$

This mirrors the logic used in Theorem 2.1. Checking the curvature of the Hamiltonian in terms of $u$ allows one to determine whether the problem concerns maximization or minimization. Specifically:

If

$$\frac{\partial^2 \mathcal{H}}{\partial u^2} < 0 \; at \; u^*, \tag{2.2.9}$$

then the problem is maximization, Conversely, if

$$\frac{\partial^2 \mathcal{H}}{\partial u^2} > 0 \; at \; u^*, \tag{2.2.10}$$

the problem is minimization.

This second-order condition provides a useful tool for verifying whether a candidate control leads to a local extremum, supplementing the first-order optimality conditions derived from the Hamiltonian.



doi:10.6342/NTU202501357

## 2.3 Bang-Bang Control

Consider the following OCP

$$\begin{aligned} \max_{u} \quad & \int_{t_0}^{t_1} [f_1(t,x) + u(t) f_2(t,x)] dt \\ subject\ to \quad & x'(t) = g_1(t,x) + u(t) g_2(t,x) \\ & x(0) = x_0, \ \ m \le u(t) \le n. \end{aligned} \tag{2.3.1}$$

The corresponding Hamiltonian is given by:

$$\mathcal{H} = f_1(t,x) + u(t) f_2(t,x) + \lambda(t)[g_1(t,x) + u(t) g_2(t,x)]. \tag{2.3.3}$$

The adjoint equation, derived from the necessary condition $\lambda'(t) = -\frac{\partial \mathcal{H}}{\partial x}$ follows the standard form. The optimality condition in terms of the control variable yields:

$$\frac{\partial \mathcal{H}}{\partial u} = f_2(t,x) + \lambda(t) g_2(t,x), \tag{2.3.3}$$

Since this expression lacks an explicit solution for $u$. we define the $\Psi(t)$ as $\Psi(t) = f_2(t,x) + \lambda(t) g_2(t,x)$. Based on the sign of $\Psi(t)$, the optimal control $u^*$ can be characterized as:

$$u^*(t) = \begin{cases} m \ if \ \Psi(t) < 0 \\ ? \ if \ \Psi(t) = 0 \\ n \ if \ \Psi(t) > 0 \end{cases}. \tag{2.3.4}$$

When $\Psi = 0$ occurs only at isolated time instances and not over intervals, the control $u^*(t)$ exhibits what is known as bang-bang behavior. In such cases, the control switches abruptly between its lower and upper bounds $m$ and $n$, resulting in a piecewise constant control function. These discontinuities in control correspond to switching times, i.e., points where the sign of $\Psi(\mathrm{t})$ changes. While the exact control value at the switching time is often not uniquely determined, what matters more is the timing of these transitions, as they represent key moments for adjusting the control strategy. Figure 2-2 provides a graphical illustration of such a bang-bang control



doi:10.6342/NTU202501357

profile.

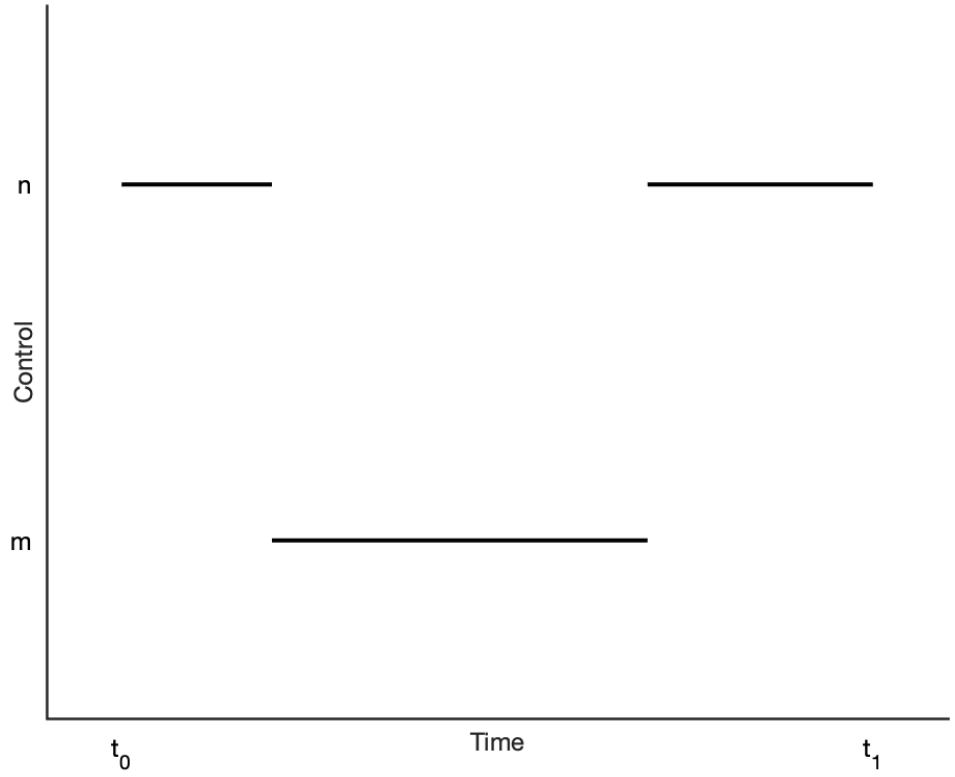


Figure 2-2 A typical bang-bang control.

## 2.4 Payoff Terms

In many OCP, the objective extends beyond optimizing a performance index over the entire time horizon—it may instead emphasize the system's state at a specific moment, typically at the terminal time. For example, in cancer therapy models, the aim is often to minimize the number of tumor cells by the end of the treatment period. Similarly, epidemic management strategies may prioritize reducing the number of infected individuals at the conclusion of the intervention. In the earlier example, Eq. (2.1.4) focuses on maximizing the bacterial population at the final time. To appropriately address goals of this type, it becomes necessary to adapt the standard



doi:10.6342/NTU202501357

optimality conditions to explicitly account for terminal-state contributions. A general formulation of such problems is given by:

$$\begin{aligned} &\max_{u}[\varphi\big(x(t_1)\big) + \int_{t_0}^{t_1} f\big(t, x(t), u(t)\big)dt] \\ &\textit{subject to} \quad x'(t) = g\big(t, x(t), u(t)\big) \\ &\qquad\qquad x(t_0) = x_0, \end{aligned} \tag{2.4.1}$$

where $\varphi\big(x(t_1)\big)$ denotes a terminal-state objective, often referred to as a payoff term or salvage term. Accordingly, the OF becomes:

$$J(u) = \int_{t_0}^{t_1} f\big(t, x(t), u(t)\big)dt + \varphi\big(x(t_1)\big). \tag{2.4.2}$$

To derive the necessary condition, we consider the variation in $J(u^{\epsilon})$ around the optimal control $u^{*}$, leading to:

$$0 = \lim_{\epsilon \to 0} \frac{J(u^{\epsilon}) - J(u^{*})}{\epsilon}. \tag{2.4.3}$$

The key modification, compared to the case without a terminal objective, arises in the boundary condition at the final time. Specifically, the resulting variation of the OF yields:

$$\begin{aligned} 0 = \int_{t_0}^{t_1} \Big[(f_x + \lambda g_x + \lambda') \frac{dx^{\epsilon}}{d\epsilon}\Big|_{\epsilon=0} + (f_u + \lambda g_u)h\Big] dt - \big(\lambda(t_1) - \\ \varphi'^{(x(t_1))}\big) \frac{dx^{\epsilon}}{d\epsilon}(t_1)\Big|_{\epsilon=0}. \end{aligned} \tag{2.4.4}$$

which introduces an additional term at $t = t_1$ due to the presence of the terminal payoff.

Accordingly, if the adjoint variable $\lambda(t)$ is chosen to satisfy both the previously derived adjoint differential equation and the modified terminal condition:

$$\lambda'(t) = -f_x(t, x^{*}, u^{*}) - \lambda(t) g_x(t, x^{*}, u^{*}), \tag{2.4.5}$$

$$\lambda(t_1) = \varphi'\big(x^{*}(t_1)\big), \tag{2.4.6}$$



doi:10.6342/NTU202501357

then the variational expression in Eq. (2.4.4) simplifies to:

$$0 = \int_{t_0}^{t_1} (f_u + \lambda g_u) h dt, \tag{2.4.7}$$

As this holds for all admissible variation functions $h(t)$ the optimality condition becomes:

$$f_u(t, x^*, u^*) - \lambda g_u(t, x^*, u^*) = 0. \tag{2.4.8}$$

All other necessary conditions, including the state equation and the adjoint dynamics, remain unchanged. The only adjustment is the updated transversality condition at the final time, presented in Eq. (2.4.6). This modification systematically incorporates objectives that depend explicitly on the terminal state, ensuring such problems—where a payoff term is present—are properly addressed within the optimal control structure.

## 2.5 Bounded Controls

In many real-world applications, it is essential to impose constraints on the control variable to ensure that the resulting solution is physically meaningful. For instance, when the control represents the quantity of a chemical substance introduced into a system, it must remain nonnegative—i.e., $u \geq 0$ Moreover, there may exist an upper bound due to physical limitations or regulatory guidelines governing chemical usage. Similarly, when the control denotes a proportion—such as the fraction of effort, muscular force, or resource allocation—it is often appropriate to constrain it within a normalized interval, typically $0 \leq u \leq 1$. These bounds serve to reflect practical limitations and are crucial for ensuring that the control strategy remains feasible and interpretable within its intended context.



doi:10.6342/NTU202501357

### 2.5.1 Necessary Conditions

To address OCPs that involve bounded controls, we introduce an alternative set of necessary conditions. Consider the following formulation:

$$\begin{aligned} &\max_{u}[\varphi\big(x(t_1)\big) + \int_{t_0}^{t_1} f\big(t, x(t), u(t)\big)dt] \\ &subject\ to \quad x'(t) = g\big(t, x(t), u(t)\big) \\ &x(t_0) = x_0, \qquad m \le u(t) \le n. \end{aligned} \tag{2.5.1}$$

Where $m$ and $n$ are fixed real constants satisfying $n > m$. Define $J(u)$ as the OF associated with control input $u$, and let $x = x(u)$ denote the corresponding state trajectory. Then:

$$J(u) = \varphi\big(x(t_1)\big) + \int_{t_0}^{t_1} f\big(t, x(t), u(t)\big)dt. \tag{2.5.2}$$

Assume $(x^*, u^*)$ is an optimal solution pair. Suppose $h(t)$ be a piecewise continuous perturbation function, for which there exists a positive constant $\epsilon_0$, such that for all $\epsilon \in (0, \epsilon_0), u^{\epsilon}(t) = \epsilon h(t) + u^*(t)$ remains admissible—i.e., it satisfies the constraint:

$$m \le u^{\epsilon}(t) \le n\ for\ all\ t. \tag{2.5.3}$$

Due to the constraints placed on the control variable, the derivative of the OF in terms of the control may not necessarily vanish at the optimal solution. This situation arises when the optimal control $u^*(t)$ attains either its upper or lower bound at specific time instances. Under such circumstances, it is no longer appropriate to enforce a zero-derivative condition; instead, we assess the sign of the derivative to infer optimality. To accurately determine this sign, we must also impose a restriction on the sign of the perturbation parameter denote the state trajectory associated with the perturbed control $u^{\epsilon}(t) = \epsilon h(t) + u^*(t)$ for each $\epsilon \in (0, \epsilon_0)$, By applying the



doi:10.6342/NTU202501357

Fundamental Theorem of Calculus and introducing a piecewise differentiable adjoint function $\lambda(t)$ we can express the OF $J(u^\epsilon)$ in the form:

$$J(u^\epsilon) = \int_{t_0}^{t_1} [f(t, x^\epsilon, u^\epsilon) + \lambda(t) g(t, x^\epsilon, u^\epsilon) + x^\epsilon(t)\lambda'(t)]dt - \lambda(t_0)x_0 + \lambda(t_0)x^\epsilon(t_1) + \varphi\big(x(t_1)\big). \tag{2.5.4}$$

Since the $J(u)$ reaches its maximum at the optimal control $u^*$ the directional derivative with respect to any admissible variation must be non-positive. That is,

$$0 \geq \frac{d}{d\epsilon} J(u^\epsilon)\Big|_{\epsilon=0} = \lim_{\epsilon \to 0^+} \frac{J(u^\epsilon) - J(u^*)}{\epsilon} \tag{2.5.5}$$

Here, $\epsilon$ is chosen to be positive, ensuring the perturbed control $u^\epsilon = \epsilon h + u^*$ remains within the admissible set. Since $u^*$ maximizes $J$, the numerator must be non-positive, and therefore the entire expression does not exceed zero. Consequently, the variational inequality becomes:

$$0 \geq \int_{t_0}^{t_1} (f_u + \lambda g_u) h dt, \tag{2.5.6}$$

This result is derived under the assumption that the adjoint variable $\lambda(t)$ satisfies the following relations:

$$\lambda'(t) = -f_x(t, x^*, u^*) - \lambda(t) g_x(t, x^*, u^*), \tag{2.5.7}$$

$$\lambda(t_1) = \varphi'\big(x^*(t_1)\big). \tag{2.5.8}$$

Now, consider a point $s \in [t_0, t_1]$ where $u^*(s)$ is continuous and satisfies $m \leq u^*(s) \leq n$. Suppose $f_u + \lambda g_u > 0$. By continuity of $u^*$ and the integrand, there exists a neighborhood $I$ of $s$ such that the same inequality holds over all $t \in I$ and $u^*(t) < n$. Let

$$M = \max\{u^*(t) : t \in I\} < b. \tag{2.5.9}$$

Define the variation function $h(t)$ as:



doi:10.6342/NTU202501357

$$h(t) = \begin{cases} n - M & if \quad t \in I \\ 0 & otherwise \end{cases}. \tag{2.5.10}$$

Clearly, $h > 0$ on $I$, or all $\epsilon \in [0,1]$, the perturbed control $u^{\epsilon}(t) = u^{*}(t) + \epsilon h$ remains within the bounds$[m, n]$. However, this leads to:

$$\int_{t_0}^{t_1} (f_u + \lambda g_u) h dt = \int_{I}^{\square} (f_u + \lambda g_u) h dt > 0, \tag{2.5.11}$$

which contradicts Eq. (2.5.6), implying that the assumption $f_u + \lambda g_u \geq 0$ at $s$ must be false. Thus, it follows that $f_u + \lambda g_u \leq 0$. Suppose $f_u + \lambda g_u < 0$ at point of continuity $s$ where $m < u^{*}$ Then, a neighborhood $I$ exists where $f_u + \lambda g_u < 0$ and $u^{*} > a$ for all $t \in I$. Let

$$M = \min\{u^{*}(t) : t \in I\} \tag{2.5.12}$$

and define $h = a - m$ on $I$ and 0 off $I$. Again, $u^{*}(t) + \epsilon h \in [m, n]$ for all $\epsilon \in [0,1]$. But this gives

$$\int_{t_0}^{t_1} (f_u + \lambda g_u) h dt = \int_{I}^{\square} (f_u + \lambda g_u) h dt > 0, \tag{2.5.13}$$

again contradicts Eq. (2.5.6), Thus, the inequality must reverse: $f_u + \lambda g_u \geq 0$ at $s$. Putting both results together, we conclude that at any continuity point $s$ of $u^{*}$, the following complementary slackness condition holds:

$$\begin{array}{lll} u^{*}(t) = m & implies & f_u + \lambda g_u \leq 0 \; at \; t, \\ m < u^{*}(t) < n & implies & f_u + \lambda g_u = 0 \; at \; t, \\ u^{*}(t) = n & implies & f_u + \lambda g_u \geq 0 \; at \; t. \end{array} \tag{2.5.14}$$

The conditions in Eq. (2.5.14) are equivalent to the following characterizations of the optimal control $u^{*}(t)$ at all points of continuity.

$$\begin{array}{lll} f_u + \lambda g_u \leq 0 \; at \; t & implies & u^{*}(t) = m, \\ f_u + \lambda g_u = 0 \; at \; t & implies & m < u^{*}(t) < n, \\ f_u + \lambda g_u \geq 0 \; at \; t & implies & u^{*}(t) = n. \end{array} \tag{2.5.15}$$

This set of conditions holds almost everywhere, as discontinuity points of $u^{*}(t)$. are



doi:10.6342/NTU202501357

of measure zero and do not influence the OF or the system dynamics. Thus, they may be excluded from consideration in the derivation of necessary conditions. The construction of the Hamiltonian function remains unchanged:

$$\mathcal{H}(t,x,u,\lambda) = f(t,x,u) + \lambda(t)g(t,x,u), \tag{2.5.16}$$

The dynamics of the state and adjoint variables follow the standard form:

$$x'(t) = \frac{\partial \mathcal{H}}{\partial \lambda}, \qquad x(t_0) = x_0, \tag{2.5.17}$$

$$\lambda'(t) = -\frac{\partial \mathcal{H}}{\partial x}, \qquad \lambda(t_1) = \varphi'\big(x^*(t_1)\big). \tag{2.5.18}$$

Based on the optimality condition derived earlier, the control $u^*(t)$ satisfies:

$$\begin{cases} u^* = m & if \quad \dfrac{\partial \mathcal{H}}{\partial u} < 0 \\ m < u^*(t) < n & if \quad \dfrac{\partial \mathcal{H}}{\partial u} = 0 \\ u^* = n & if \quad \dfrac{\partial \mathcal{H}}{\partial u} > 0 \end{cases}. \tag{2.5.19}$$

These results correspond to a bounded-control version of PMP, where the maximization of the Hamiltonian is constrained to the admissible control set $m \le u \le n$. For minimization problems, the direction of the inequalities in Eq. (2.5.19) is reversed accordingly. It is important to note that the presence of control constraints does not modify the transversality condition. The necessary conditions outlined above are derived under the assumption that the initial state is fixed, while the terminal state remains free.



doi:10.6342/NTU202501357

# Chapter 3 Materials and Methods

## 3.1 Background of Fitness-Fatigue Model

### 3.1.1 Introduction to Fitness-Fatigue Model

The performance model adopted in the optimal control formulation of this study is derived from the FFM. This section introduces the FFM along with relevant background concepts, providing a theoretical basis for constructing the optimal control formulation used in our analysis.

In 1975, Banister et al. [20] proposed that athletic performance responses to training stimuli could be characterized using a first-order dynamic system, represented by the following model:

$$PER'(t) = -\frac{1}{\eta}PER(t) + kTR(t), \tag{3.1.1}$$

In this model, $PER(t)$ denotes athletic performance at time $t$, $\eta$ is the time constant, $k$ is the gain coefficient, and $TR(t)$ represents the training load (commonly referred to as TRIMP) at time $t$. $\eta$ and $k$ reflect individual physiological characteristics. Here, $PER(t)$ serves as the model output—that is, the predicted performance level—while $TR(t)$ functions as the training stimulus. In experimental settings, $TR(t)$ is typically calculated from empirical data using researcher-defined formulas, which may vary between studies [25, 32].

Originally referred to as the Banister IR model and expressed in Eq. (3.1.1), this formulation captures the temporal decline in performance in the absence of training, while also illustrating how appropriately timed training stimuli can delay or reverse this decline. The model attempts to quantify the effect of training load on performance but does not



doi:10.6342/NTU202501357

account for other influential variables such as sleep quality [44], nutrition [44, 45], psychological stress [45], injury, illness, or environmental conditions [45].

In 1976, Calvert et al. [21] introduced a mathematical procedure for analyzing Eq. (3.1.1) By applying the Laplace transform to the Banister formulation, the expression becomes:

$$\mathcal{L}\{PER'(t)\} = \mathcal{L}\left\{-\frac{1}{\eta}PER(t) + kTR(t)\right\}, \tag{3.1.2}$$

which leads to

$$s\overline{PER}(s) - PER(0) = -\frac{\overline{PER}(s)}{\eta} + k\overline{TR}(s), \tag{3.1.3}$$

where $s$ is the Laplace variable, and $\overline{PER}(s)$, and $\overline{TR}(s)$ denote the Laplace transforms of $PER(t)$ and $TR(t)$, respectively. Assuming a zero initial performance, i.e., $PER(0) = 0$, this simplifies to

$$\overline{PER}(s) = \frac{k\overline{TR}(s)}{s + \frac{1}{\eta}}. \tag{3.1.4}$$

Letting $\bar{G}(s) = \frac{1}{s+\frac{1}{\eta}}$, Eq. (3.1.4) becomes

$$\overline{PER}(s) = k\bar{G}(s)\overline{TR}(s). \tag{3.1.5}$$

By the convolution theorem, taking the inverse Laplace transform of both sides gives

$$\mathcal{L}^{-1}[\overline{PER}(s)] = \mathcal{L}^{-1}[k\bar{G}(s)\overline{TR}(s)] = k\mathcal{L}^{-1}[\bar{G}(s)\overline{TR}(s)] = k(G * TR)(t), \tag{3.1.6}$$

or

$$PER(t) = k\int G(t-\Theta)\,TR(\Theta)d\Theta, \tag{3.1.7}$$

assume $-a = \frac{1}{\eta}$, then $G(t) = \mathcal{L}^{-1}[\bar{G}(s)] = e^{-\frac{t}{\eta}}$. Therefore



doi:10.6342/NTU202501357

$$PER(t) = k \int e^{\frac{-(t-\Theta)}{\eta}} TR(\Theta) d\Theta, \tag{3.1.8}$$

To facilitate numerical implementation, the integral form is discretized as

$$PER(t) = k \sum_{i=1}^{t-1} e^{\frac{-(t-i)}{\eta}} TR(i)\,\Delta t = k \sum_{i=1}^{t-1} e^{\frac{-(t-i)}{\eta}} TR(i), \tag{3.1.9}$$

where a unit time interval $\Delta t = 1$ is assumed. Here, $PER(t)$ represents the cumulative training effect up to day $t$, while $TR(i)$ denotes the training impulse on day $i$. Extending this formulation to account for both positive (fitness) and negative (fatigue) components, the performance is modeled as

$$PER(t) = PER(0) + k_1 \sum_{i=0}^{t-1} e^{-\frac{t-i}{\eta_1}} TR(i) - k_2 \sum_{i=0}^{t-1} e^{-\frac{t-i}{\eta}} TR(i), \tag{3.1.10}$$

which forms the classical FFM.

To simultaneously represent the opposing effects of training—namely, the enhancement of fitness and the accumulation of fatigue—Turner et al. [29] proposed a refined dynamical system described by

$$\begin{aligned} FIT'(t) &= -\frac{1}{\eta_1} FIT(t) + k_1 TR(t), \\ FAT'(t) &= -\frac{1}{\eta_2} FAT(t) + k_2 TR(t), \\ PER(t) &= PER(0) + FIT(t) - FAT(t), \end{aligned} \tag{3.1.11}$$

where $TR(t)$, $FAT(t)$, $FIT(t)$, and $PER(t)$ denote, respectively, the TRIMP, fatigue, fitness and performance at time $t$. The constants $\eta_1$, $\eta_2$, $k_1$ and $k_2$ characterize individual physiological responses, with $\eta_1$ and $\eta_2$ representing time constants and $k_1$ and $k_2$ serving gain factors. The initial performance level is denoted by $PER(0)$. The first two differential equations describe the dynamic accumulation and decay of fitness



doi:10.6342/NTU202501357

and fatigue in response to training input, while the third equation models performance as the net result of these two factors superimposed on the baseline level. This formulation aligns with the commonly accepted interpretation that training improves performance through fitness gains, yet simultaneously impairs it via fatigue accumulation. This system of equations serves as the dynamic model in our optimal control formulation, providing the foundation to simulate and optimize performance trajectories over time.

### 3.1.2 Definition and Measurement of Fitness, Fatigue, Performance, and TRIMP

In this subsection, we introduce the definitions of four central constructs in performance modeling: fitness, fatigue, performance, and TRIMP, along with a brief discussion of their typical measurement approaches.

While numerous physiological indicators and subjective questionnaire scores have been found to correlate to varying extents with fitness and fatigue within the context of the FFM and its derivatives, no single measurable variable can fully capture the dynamic nature of either construct. This limitation arises because both fitness and fatigue are conceptual representations of the cumulative influence of multiple internal and external factors that collectively shape athletic performance over time.

Consequently, most empirical studies utilizing the FFM or its variants do not attempt to measure fitness and fatigue directly. Instead, researchers typically collect objective performance outcomes—such as time, distance, velocity, or power output—and fit these data to the model. Once the model parameters are calibrated, the latent trajectories of fitness and fatigue can then be inferred retrospectively.



doi:10.6342/NTU202501357

TRIMP is commonly defined as the product of training intensity and session duration. Several formulations have been proposed to quantify TRIMP, encompassing both external training loads (e.g., running distance, speed, power output) and internal training loads, which reflect the athlete's physiological or perceptual responses (e.g., heart rate, rating of perceived exertion). Among these, the Banister TRIMP and its subsequent adaptations remain the most widely used and validated methods for estimating training load in the literature [46].

The Banister TRIMP is calculated using the equation

$$\text{TRIMP} = t \times c \times \Delta\text{HR}, \tag{3.1.12}$$

where $t$ represents the length of the training session (in minute), and $c$ is a sex-specific scaling factor that accounts for the exponential relationship between heart rate response and exercise intensity. For male athletes, $c = 0.64e^{1.92\times\Delta\text{HR}}$, whereas for female athletes, $c = 0.86e^{1.67\times\Delta\text{HR}}$. The term $\Delta\text{HR} = \frac{\text{HR}_{\text{average}}-\text{HR}_{\text{rest}}}{\text{HR}_{\text{max}}-\text{HR}_{\text{rest}}}$ represents the proportion of heart rate reserve utilized during the session, where $\text{HR}_{\text{average}}$ and $\text{HR}_{\text{max}}$ denote the average and maximum heart rates recorded during the session, and $\text{HR}_{\text{rest}}$ is the athlete's resting heart rate. This formulation captures both the duration and physiological intensity of training, thereby providing a composite measure of internal training load.

The Edwards TRIMP (eTRIMP) is a kind of modified TRIMP. To calculate eTRIMP, five zones are defined according to the percentage of $\text{HR}_{\text{max}}$: "Zone 1 (50–59% $\text{HR}_{\text{max}}$), Zone 2 (60–69% $\text{HR}_{\text{max}}$), Zone 3 (70–79% $\text{HR}_{\text{max}}$), Zone 4 (80–89% $\text{HR}_{\text{max}}$), and Zone 5 (90–100% $\text{HR}_{\text{max}}$)". The equation for calculating eTRIMP is

$$\text{eTRIMP} = \sum_{i=1}^{5} \text{IF}_i \times t_i \times c \times \Delta\text{HR}_i, \tag{3.1.13}$$



doi:10.6342/NTU202501357

where $\mathrm{IF}_i$ is a scaling constant equal to 1, 2, 3, 4 and 5 for each zone, respectively. $t_i$ is the time duration in each zone. $\Delta\mathrm{HR}_i = \frac{\mathrm{HR_{average}} - \mathrm{HR_{rest}}}{\mathrm{HR_{max,i}} - \mathrm{HR_{rest}}}$ is the fraction of HR in each zone, where $\mathrm{HR_{max,I}}$ is the maximum HR in each zone.

The Lucia TRIMP (luTRIMP) is another refined variation of the original TRIMP concept, designed to incorporate metabolic thresholds rather than heart rate zones for quantifying internal training load. This method divides exercise intensity into three physiologically meaningful zones based on gas exchange threshold (GET) and the respiratory compensation point (RCP), which are commonly identified through cardiopulmonary exercise testing (CPET). The zones are defined as follows: “zone 1, below GET; zone 2, between GET and RCP; zone 3, above RCP”.

Each zone is associated with a corresponding weighting factor that reflects the increasing physiological stress and internal load. The luTRIMP is calculated as:

$$\mathrm{luTRIMP} = \sum_{i=1}^{3} \mathrm{IF}_i \times t_i \times c \times \Delta\mathrm{HR}, \tag{3.1.14}$$

where $\mathrm{IF}_i$ is a scaling constant equal to 1, 2 and 3 for each zone, respectively. $t_i$ is the time duration in each zone.

In addition to the TRIMP-based metrics described earlier, several alternative methods have been developed to quantify training load based on either subjective perception or mechanical output. Three such metrics are introduced below.

First, the session rating of perceived exertion (sRPE) is a widely used subjective measure. After completing a training session, the athlete reports their perceived exertion using the CR-10 scale**.** The sRPE is then computed as:

$$sRPE = RPE \times t, \tag{3.1.15}$$



doi:10.6342/NTU202501357

where $t$ represents the duration of the session (in minutes). This method captures the athlete's internal perception of the training stress and integrates it with session duration to provide a holistic load estimate.

Second, the Training Stress Score (TSS) is an objective metric commonly used in endurance sports, particularly cycling. It accounts for both the intensity and duration of the session, and is defined as:

$$\mathrm{TSS} = \frac{t \times \mathrm{NP} \times \mathrm{IF}}{\mathrm{FTP} \times 3600} \times 100, \tag{3.1.16}$$

where $t$ is the time of the training session duration and $\mathrm{NP}$ is the normalized power. $\mathrm{IF}$ is equal to $\frac{\mathrm{NP}}{\mathrm{FTP}}$, where $\mathrm{FTP}$ is the functional threshold power of the subject. TSS reflects the relative difficulty of a workout compared to a one-hour maximal effort.

Lastly, mechanical energy expenditure is a purely external load indicator, computed as the total amount of work performed during the training session. This is given by:

$$\text{Energy expenditure} = \text{Power} \times \text{Time}. \tag{3.1.17}$$

This metric provides a direct measurement of the mechanical work performed, typically expressed in kilojoules, and is particularly useful when analyzing sessions involving constant or steady-state output.



doi:10.6342/NTU202501357

## 3.2 Optimal Control Framework: Mathematical Formulation and Computational Solution

### 3.2.1 Applying Optimal Control Theory to Fitness-Fatigue Model

This subsection shows the formulated optimal control framework and its corresponding solution methods.

The dynamic relationship among fitness, performance, fatigue, and TRIMP is described by Eq. (3.1.11), which provides a physiologically meaningful basis for designing personalized training strategies. The primary objective is to maximize athletic performance on the competition day by promoting fitness accumulation while simultaneously minimizing fatigue. In addition, the framework aims to control the total accumulated TRIMP over the training period, thereby reducing the risk of overtraining and injury due to excessive load. Effective TRIMP management is critical not only for maintaining optimal physiological and psychological conditions, but also for ensuring long-term training sustainability. An additional motivation for minimizing TRIMP, without compromising final performance, lies in its practical implications: achieving similar or improved performance outcomes with reduced training volume enables athletes to allocate more time and energy to recovery, personal commitments, or other life domains, thus contributing to enhanced overall well-being and quality of life.

Accordingly, the OF is formulated as follows:

$$\max_{m}\left[FIT(t_p) - FAT(t_p) - A\int_0^{t_p} TR^2(t)dt\right], \tag{3.2.1}$$

where $t_p$ denotes the length of the training period (in days) up to the competition, while $A$ is a weighting parameter that regulates the trade-off between performance maximization and TRIMP minimization. The parameter $A$ governs both the peak



doi:10.6342/NTU202501357

intensity of training (i.e., the highest daily TRIMP) and the number of high-intensity training days within the training horizon. The simulation assumes these values to remain unchanged. Chapter 4 will offer an in-depth discussion on the interpretation and applied significance of $A$.

Combining Eqs. (3.1.11) and (3.2.1), the OCP is formulated as

$$\max_{TR}\left[FIT(t_p) - FAT(t_p) - A\int_0^{t_p} TR^2(t)dt\right] \tag{3.2.2}$$

*subject to*

$$FIT'(t) = -\frac{1}{\eta_1}FIT(t) + k_1 TR(t), FIT(0) = 0, \tag{3.2.3}$$

$$FAT'(t) = -\frac{1}{\eta_2}FAT(t) + k_2 TR(t), FAT(0) = 0, \tag{3.2.4}$$

$$M_1 \le TR(t) \le M_2, \tag{3.2.5}$$

$$PER(t) = PER(0) + FIT(t) - FAT(t), PER(0) = 0. \tag{3.2.6}$$

$M_1$ and $M_2$ represent the lower and upper restricts of the control variable $TR(t)$, respectively. Assume that the control signal is defined in a piecewise continuous manner, and the state variables maintain continuity throughout. Although the parameters and variables in our formulated control approach may be expressed in any appropriate units depending on the application context, the present study adopts the following unit conventions: $\eta_1$ and $\eta_2$ are time-decay constants (units: days), and $k_1$ and $k_2$ are dimensionless gain factors.; The control variable $TR(t)$, representing training load, is modeled as a percentage of maximum sustainable effort and restricted to a bounded interval, typically [0, 100], where the lower bound $M_1$ is 0 and the upper bound $M_2$ is 100. The variables $FIT(t)$, $PER(t)$ and $FAT(t)$ are measured in arbitrary units. To guarantee our OCP exist solution and the result unique, a rigorous proof will be provided in Section 3.2.2.



doi:10.6342/NTU202501357

### 3.2.2 The Proof of Existence and Uniqueness Results

To finalize the proof, we introduce several definitions and theorems derived from Lenhart and Workman [38], particularly referencing Definition 1.4, Theorem 2.1, and Theorem 2.2.

**DEFINITION 3.1**

*Let* $f(x)$ *be a function defined on the interval* $I$*. The function* $f(x)$ *is said to be strictly concave if, for every* $a, b \in I$*, and for all* $c \in (0,1)$*, the following inequality holds:*

$$f\big((1-c)a + \lambda b\big) > (1-c)f(a) + \lambda f(b).$$

**THEOREM 3.1**

*Consider the OCP defined as*

$$J(w) = \max_{w}\left[\int_{t_0}^{t_1} f\big(t, x_1(t), \dots, x_n(t), TR(t)\big)dt\right] + \varphi\big(x_1(t_1), \dots, x_n(t_1)\big) \qquad (3.2.7)$$

*subject to*

$$x_i'(t) = g_i\big(t, x_1(t), \dots, x_n(t), TR(t)\big), \qquad (3.2.8)$$

$$x_i(t_0) = x_{i0}, for\ i = 1, 2, \dots, n \qquad (3.2.9)$$

*where the functions* $f$ *and* $g_i$ *continuously differentiable with respect to all their variables, and are concave in both* $x_n$ *and* $m$*. Suppose that* $TR$ *is an optimal control with corresponding state trajectory* $x_n^*$ *and an associated piecewise differentiable adjoint function* $\lambda_n$ *such that* $t_0 \le t \le t_1$*, the following conditions hold:*

$$f_{TR} + \lambda_n g_{TR} = 0, \qquad (3.2.10)$$



doi:10.6342/NTU202501357

$$\lambda_n' = -\left(f_{x_n} + \lambda_n g_{x_n}\right),$$

$$\lambda_n(t_1) = \varphi'\left(x_n(t_1)\right),$$

$$\lambda_n(t) \geq 0.$$

*Then, for any admissible control* $TR$*, the optimality condition*

$$J(TR^*) \geq J(TR). \tag{3.2.11}$$

**THEOREM 3.2**

*Consider the control set to be the space of Lebesgue integrable functions defined on the interval* $[t_0, t_1]$ *with values in* $\mathbb{R}$*. Assume that the function* $f\left(t, x_1(t), \dots, x_n(t), TR(t)\right)$ *is concave in the control variable* $TR$*. Furthermore, suppose there exist positive constants* $C_4$ *and* $C_1, C_2, C_3 > 0$ *and a real number* $\beta > 1$ *such that for each* $i$*,*

$$\begin{gathered} g_i\left(t, x_1(t), \dots, x_n(t), TR(t)\right) = \alpha(t, x_n) + \beta(t, x)TR, \\ \left|g_i\left(t, x_1(t), \dots, x_n(t), TR(t)\right)\right| \leq C_1(1 + |x_n| + |TR|), \\ g_i\left(t, x_1(t), \dots, x_n(t), TR(t)\right) - g\left(t, x(t), TR(t)\right) \leq C_2|x_1 - x|(1 + |TR|), \\ f\left(t, x_1(t), \dots, x_n(t), TR(t)\right) \geq C_3|TR|^{\beta} - C_4. \end{gathered} \tag{3.2.12}$$

*Under these assumptions, there exists an optimal control* $TR^*$ *that maximizes the OF* $J(TR)$*, and the value* $J(TR^*)$ *is finite.*

Firstly, we establish that the OF $J(TR)$ is concave in terms of the control variable $TR$. The OF in this OCP is given by

$$J\left(TR(t)\right) = FIT\left(t_p\right) - FAT\left(t_p\right) + I\left(TR(t)\right), \tag{3.2.13}$$

where



doi:10.6342/NTU202501357

$$I\big(TR(t)\big) = -A\int_0^{t_p} TR^2(t)dt. \tag{3.2.14}$$

Consider any two admissible controls $TR_2(t)$ and $TR_1(t)$ and their convex combination

$$TR_c(t) = cTR_1(t) + (1-c)TR_2(t), \text{where } c \in (0,1). \tag{3.2.15}$$

Substituting $TR_c(t)$ into Eq. (3.2.14), we obtain

$$\begin{aligned} I\big(TR_c(t)\big) &= -A\int_0^{t_p} \big(cTR_1(t) + (1-c)TR_2(t)\big)^2 dt \\ &= -A\int_0^{t_p} (c^2\big(TR_1(t)\big)^2 + 2c(1-c)TR_1(t)TR_2(t) \\ &\quad + (1-c)^2\big(TR_2(t)\big)^2)dt. \end{aligned} \tag{3.2.16}$$

On the other hand, the convex combination of the functionals is

$$\begin{aligned} &cI(TR_1(t)) + (1-c)I\big(TR_2(t)\big) \\ &= -A\int_0^{t_p} \Big(c\big(TR_1(t)\big)^2 + (1-c)\big(TR_2(t)\big)^2\Big)dt. \end{aligned} \tag{3.2.17}$$

Subtracting Eq. (3.2.17) from Eq. (3.2.16) yields

$$\begin{aligned} &I\big(TR_c(t)\big) - \Big(cI(TR_1(t)) + (1-c)I\big(TR_2(t)\big)\Big) \\ &= Ac(1-c)\int_0^{t_p} \big(TR_1(t) - TR_2(t)\big)^2 dt. \end{aligned} \tag{3.2.18}$$

Since $A > 0$, $c(1-c) > 0$ and $\big(TR_1(t) - TR_2(t)\big)^2 > 0$ Eq. (3.2.18) guarantees that

$$I\big(TR_c(t)\big) - \Big(c(TR_1(t)) + (1-c)I\big(TR_2(t)\big)\Big) > 0, \forall TR_1 \neq TR_2. \tag{3.2.19}$$

According to Definition 3.1, Eq. (3.2.19) demonstrates that $I\big(TR_c(t)\big)$ in the OF is strictly concave. Since $FAT\big(t_p\big)$ and $FIT\big(t_p\big)$ are constants with respect to the control, the entire OF $J\big(TR(t)\big) = -FAT\big(t_p\big) + FIT\big(t_p\big) + I\big(TR(t)\big)$ is therefore strictly



doi:10.6342/NTU202501357

concave in $TR(t)$. Furthermore, $TR(t)$ is assumed to be piecewise continuous, and the state equations (Eqs. (3.2.3) and (3.2.4)) are continuously differentiable. Consequently, by Theorem 3.1, the existence and uniqueness of the solution to this OCP are guaranteed. Finally, the necessary conditions for the unique optimal control can be derived via the PMP, as will be shown in the subsequent section.

The Hamiltonian associated with our OCP is given by:

$$\mathcal{H} = -ATR^2 + \lambda_1\left(-\frac{1}{\eta_1}FIT + k_1TR\right) + \lambda_2\left(-\frac{1}{\eta_2}FAT + k_2TR\right). \tag{3.2.20}$$

The necessary conditions derived from PMP can be expressed as:

$$0 = \frac{\partial \mathcal{H}}{\partial TR} = -2ATR + k_1\lambda_1 + k_2\lambda_2 \text{ at } TR^*(t), \tag{3.2.21}$$

where $TR$(t) is the optimal control. To confirm that the problem is indeed a maximization, we examine the second-order derivative of the Hamiltonian:

$$\frac{\partial^2 \mathcal{H}}{\partial TR^2} = -2A < 0 \text{ since } A > 0. \tag{3.2.22}$$

which confirms the strict concavity of the Hamiltonian in terms of $m$, and consequently, the strict concavity of the OF $J(TR)$.

The adjoint equations are given by:

$$\lambda_1' = -\frac{\partial \mathcal{H}}{\partial FIT} = \frac{\lambda_1}{\eta_1}, \lambda_1(t_p) = 1. \tag{3.2.23}$$

$$\lambda_2' = -\frac{\partial \mathcal{H}}{\partial FAT} = \frac{\lambda_2}{\eta_2}, \lambda_2(t_p) = -1. \tag{3.2.24}$$

Solving Eqs. (3.2.23) and (3.2.24) yields:

$$\lambda_1 = e^{\frac{t-t_p}{\eta_1}} \text{ and } \lambda_2 = -e^{\frac{t-t_p}{\eta_2}}, \text{ respectively.} \tag{3.2.25}$$

The optimal control variable can be gotten by Eq. (3.2.21) as



doi:10.6342/NTU202501357

$$TR^*(t) = \frac{k_1\lambda_1 + k_2\lambda_2}{2A}. \tag{3.2.26}$$

Swapping Eq. (3.2.25) into Eq. (3.2.26), we have

$$TR^*(t) = \frac{k_1 e^{\frac{t-t_p}{\eta_1}} - k_2 e^{\frac{t-t_p}{\eta_2}}}{2A}. \tag{3.2.27}$$

Given the constraints imposed on the control variable $TR(t)$ as per Eq. (3.2.5), the admissible optimal control is:

$$TR(t) = \max\left(M_1, \min\left(\frac{k_1 e^{\frac{t-t_p}{\eta_1}} - k_2 e^{\frac{t-t_p}{\eta_2}}}{2A}, M_2\right)\right). \tag{3.2.28}$$

This expression provides a closed-form solution for the optimal control in the given OCP, derived through the application of the PMP. From Eq. (3.2.28), it is evident that $TR^*(t) \in [M_1,\ M_2]$, implying that the optimal control lies in the space $L^1([t_0, t_1, \mathbb{R}])$ i.e., the set of Lebesgue-integrable functions over the interval$[t_0,\ t_1]$. Additionally, the state variables $FIT(t_p)$ and $FAT(t_p)$ evolve according to linear ordinary differential equations in terms of $TR^*(t)$. Each state equation exhibits an affine dependence on the control input and a linear dependence on the state variables, with all associated coefficients being continuous and bounded throughout $[t_0, t_1]$. Thus, the system satisfies the standard Lipschitz and linear growth conditions, ensuring the existence and uniqueness of the state trajectories for any admissible control. Since all requirements of Theorem 3.2 are fulfilled, we conclude that an optimal control $TR^*(t)$ exists which maximizes the OF. Moreover, the analytical form of the optimal solution derived through PMP further confirms the uniqueness of the optimal solution to this OCP.



doi:10.6342/NTU202501357

### 3.2.3 The Bang-Bang Control Formulation

According to Eq. (3.2.28), the optimal TRIMP profile varies continuously over time, implying that athletes would need to adjust their training load on a daily basis. However, in real-world scenarios, training programs are usually implemented in blocks where a fixed TRIMP level is maintained for several days before transitioning to another intensity. To reflect this practical consideration, we propose an alternative OF that accommodates stepwise training patterns and aligns more closely with standard training practices.

The revised OF in our optimal control formulation is as follows

$$\max_{TR}\left[FIT(t_p) - FAT(t_p) - B\int_0^{t_p} TR(t)dt\right] \tag{3.2.29}$$

*subject to*

$$FIT'(t) = -\frac{1}{\eta_1}FIT(t) + k_1 TR(t), FIT(0) = 0, \tag{3.2.30}$$

$$FAT'(t) = -\frac{1}{\eta_2}FAT(t) + k_2 TR(t), FAT(0) = 0, \tag{3.2.31}$$

$$M_1 \le TR(t) \le M_2, \tag{3.2.32}$$

$$PER(t) = PER(0) + FIT(t) - FAT(t), PER(0) = 0. \tag{3.2.33}$$

Here, $TR(t)$ is the control variable, assumed to be piecewise continuous over the training horizon [0, $t_p$], and is expressed as a percentage of the maximum tolerable daily TRIMP, bounded by constants $M_1$ and $M_2$(e.g., 0 to 100). The state variables $FIT(t)$, $PER(t)$ and $FAT(t)$ are measured in arbitrary units. Parameters $\eta_1$, $\eta_2$ represent time constants (in days), and $k_1$, $k_2$ are dimensionless coefficients characterizing individual physiological response to training.

The Hamiltonian associated with this problem is given by:



doi:10.6342/NTU202501357

$$\mathcal{H} = -BTR + \lambda_1\left(-\frac{1}{\eta_1}FIT + k_1TR\right) + \lambda_2\left(-\frac{1}{\eta_2}FAT + k_2TR\right). \quad (3.2.34)$$

Taking the partial derivative of $\mathcal{H}$ in terms of $TR$:

$$\Psi = \frac{\partial \mathcal{H}}{\partial TR} = -B + k_1\lambda_1 + k_2\lambda_2, \quad (3.2.35)$$

the corresponding adjoint equations are:

$$\lambda_1' = -\frac{\partial \mathcal{H}}{\partial FIT} = \frac{\lambda_1}{\eta_1}, \lambda_1(t_p) = 1. \quad (3.2.36)$$

$$\lambda_2' = -\frac{\partial \mathcal{H}}{\partial FAT} = \frac{\lambda_2}{\eta_2}, \lambda_2(t_p) = -1. \quad (3.2.37)$$

Since the control does not appear explicitly in the dynamics of the adjoint variables, the structure of the optimal control is determined by the sign of $\Psi$. The points where $\Psi = 0$ re identified as switching times, indicating transitions between the upper and lower bounds of the control variable.

### 3.2.4 The Simulation Method

In Section 3.2.1 OCP, the optimal solutions $FAT^*(t)$, $TR^*(t)$ and $FIT^*(t)$ are obtained by simultaneously solving Eqs. (3.2.3), (3.2.4), (3.2.23), and (3.2.24). In Section 3.2.3 the optimal solutions $FAT(t)$, $TR^*(t)$ and $FIT^*(t)$ are similarly obtained by simultaneously solving and Eqs. (3.2.30), (3.2.31), (3.2.36), and (3.2.37).

To deal with the coupled system of equations, we employed the Forward-Backward Sweep Method [38]. Here we briefly outlined the algorithm as follows:

1. **Initialization:** An initial guess for the control variable $TR(t)$ as provided across the entire simulation interval to initiate the optimization process.



doi:10.6342/NTU202501357

2. **Forward Sweep:** Starting from the initial conditions $FAT(0) = FIT(0) = 0$, the state equations for $FIT(t)$ and $FAT(t)$ are integrated forward in time using the current estimate of $TR(t)$.
3. **Backward Sweep:** Integrate the adjoint equations for $\lambda_2(t)$ and $\lambda_1(t)$ backward in time, starting from the terminal conditions $\lambda_1(t_p) = 1$ and $\lambda_2(t_p) = -1$, with the current values of $FAT(t)$, $TR(t)$ and $FIT(t)$.
4. **Control Update:** Update $TR(t)$ by substituting the newly computed values of $FIT(t)$, $FAT(t)$, $\lambda_2(t)$ and $\lambda_1(t)$ into Eq. (3.2.22) or Eq. (3.2.36) (depends on the problem).
5. **Convergence Check:** Evaluate convergence by comparing the updated variables with those from the previous iteration. If the change in each variable is below a predefined threshold (i.e., $|current - previous| < 10^{-6}$), the algorithm terminates. Otherwise, the procedure is repeated from Step 2 until convergence is achieved.

In the forward and backward steps, any standard ordinary differential equation solver can be used. In the present study, the Runge-Kutta 4th-order method is employed as the ordinary differential equation solver. Its algorithm is described as follows. Given an ordinary differential equation $s'(t) = g(t, s(t))$, the approximation of the current $s$ value $s(t + \mathcal{E})$ is

$$s(t + \mathcal{E}) \approx s(t) + \frac{\mathcal{E}}{6}(n_1 + 2n_2 + 2n_3 + n_4), \tag{3.2.38}$$



doi:10.6342/NTU202501357

where $s(t)$ is the $s$ value of the previous iteration, $\mathcal{E}$ is the step size, $n_1 = g(t, s(t))$, $n_2 = g\left(t + \frac{\mathcal{E}}{2}, s(t) + \frac{\mathcal{E}}{2} n_1\right)$, $n_3 = g\left(t + \frac{\mathcal{E}}{2}, s(t) + \frac{\mathcal{E}}{2} n_2\right)$ and $n_4 = g(t + \mathcal{E}, s(t) + \mathcal{E} n_3)$.

For a more detailed explanation of this method, as well as information on the stability and accuracy of the fourth-order Runge-Kutta method and other variants, please refer to classical references such as Butcher's works [47, 48].

## 3.3 Simulation Setting

In this study, we pursue two primary objectives. The first is to investigate whether OCT can be effectively integrated with the FFM to achieve lower cumulative TRIMP and improved peak performance on the final day of training, compared to conventional training strategies without optimization. To this end, we adopt two sets of FFM parameters, based on values suggested in [3]. The first set is $(\eta_1, \eta_2, k_1, k_2) = (25,10,1,2)$, and the second set is $(\eta_1, \eta_2, k_1, k_2) = (30,5,1,2)$, representing different athlete profiles in terms of training response and recovery dynamics. The final training day, $t_p$ is fixed at 128 days for both sets, consistent with the configuration in [3].

During the initial phase of the investigation, we conducted three simulation experiments using OCT. In each case, the weighting parameter $A$ in Eq. (3.2.2) was set to 0.0003. To explore how the lower bound of the control variable $TR(t)$ influences the training strategy, we varied the minimum value $M_1$ is set as 0, 20 and 40 while keeping the upper bound $M_2 = 100$; This results in three distinct control ranges: $TR(t)$ is set as $0 \leq TR(t) \leq 100$, $20 \leq TR(t) \leq 100$, and $40 \leq TR(t) \leq 100$. Each simulation was solved using the numerical procedure outlined in Subsection 3.2.1, and yielded the optimal trajectories of fitness, fatigue, performance, and TRIMP across the full training



doi:10.6342/NTU202501357

period. For comparative purposes, two key performance indicators were recorded: the athlete's performance level on the final day and the cumulative TRIMP accrued over the entire training duration.

To benchmark the OCT-based results, we constructed four predefined TRIMP distributions representing typical non-optimized training regimens. These training patterns are defined as follows:

- Constant High Load: TRIMP is fixed at 100% throughout the 128-day period.
- Late Tapering: TRIMP remains at 100% for the first 120 days, then linearly decreases to 30% over the final 8 days.
- Mid-Cycle Peak: TRIMP increases linearly from 50% to 100% during the first 32 days, holds at 100% for the next 64 days, then decreases linearly back to 50% over the last 32 days.
- Symmetric Loading: TRIMP increases linearly from 0% to 100% over the first 64 days, then symmetrically decreases back to 0% over the remaining 64 days.

These TRIMP inputs were substituted into Eq. (3.1.10) to simulate performance outcomes under non-optimized control conditions. Comparing these benchmark cases with the OCT-generated training plans allows us to assess the effectiveness of optimal control in enhancing peak performance while managing overall training load.

The second objective of the study is to refine the structure of the optimized TRIMP profile. Specifically, we seek to replace the continuously varying daily TRIMP values with a stepwise pattern that more accurately reflects real-world athletic training, where training loads typically remain constant for several days before changing.

In the simulation experiments employing bang-bang control, the parameters $(\eta_1, \eta_2, k_1, k_2) = (25,10,1,2)$ were maintained. The total training duration was extended to 168 days, and three interval lengths—14, 21, and 28 days—were evaluated. For each



doi:10.6342/NTU202501357

interval length, the lower and upper bounds $M_1$ and $M_2$ were determined based on the minimum and maximum values of $TR(t)$ observed within the corresponding segments of the OCT-generated training profile. As an illustrative example, in the 14-day interval scenario, the 168-day training period was divided into 12 equal segments. Within each segment, the minimum and maximum values of $TR(t)$ from the original optimal control solution were extracted, and a bang-bang strategy was applied using only these two levels of TRIMP. This piecewise-constant control design simplifies the training plan by replacing continuously varying intensity with a binary structure, thereby making it more feasible and practical for athletes to implement in real-world settings.

In Subsection 3.2.3, we noted that for the bang-bang control problem, the switching condition is defined by setting $\Psi = 0$. Consequently, Eq. (3.2.35) reduces to the following form:

$$B = k_1\lambda_1 + k_2\lambda_2. \tag{3.3.1}$$

This relation implies that the value of $B$ directly affects the switching dynamics and thus the resulting control strategy. To select an appropriate value for $B$, we adopt the concept of the influence line**,** a method originally introduced by Fitz-Clarke et al. [49]. In their study, the influence line was used to help athletes determine the optimal timing to taper their training load for the sake of achieving peak performance on final day. Within the framework of bang-bang control, we apply the influence line similarly—to identify the ideal timing for modifying TRIMP levels. The influence line is defined by the following expression:

$$\mu = \frac{\eta_1\eta_2}{\eta_1 - \eta_2}\ln\frac{k_2}{k_1}. \tag{3.3.2}$$

Here, $\mu$ denotes the number of days before the competition on which the training load should begin to shift. Based on the parameters used in this study, the value of $\mu$ is



doi:10.6342/NTU202501357

calculated to be 11. he corresponding value of the parameter $B$ can then be selected by referencing Figure 3-1, which illustrates the relationship between $B$ and the switching dynamics governed by Eq. (3.3.1).

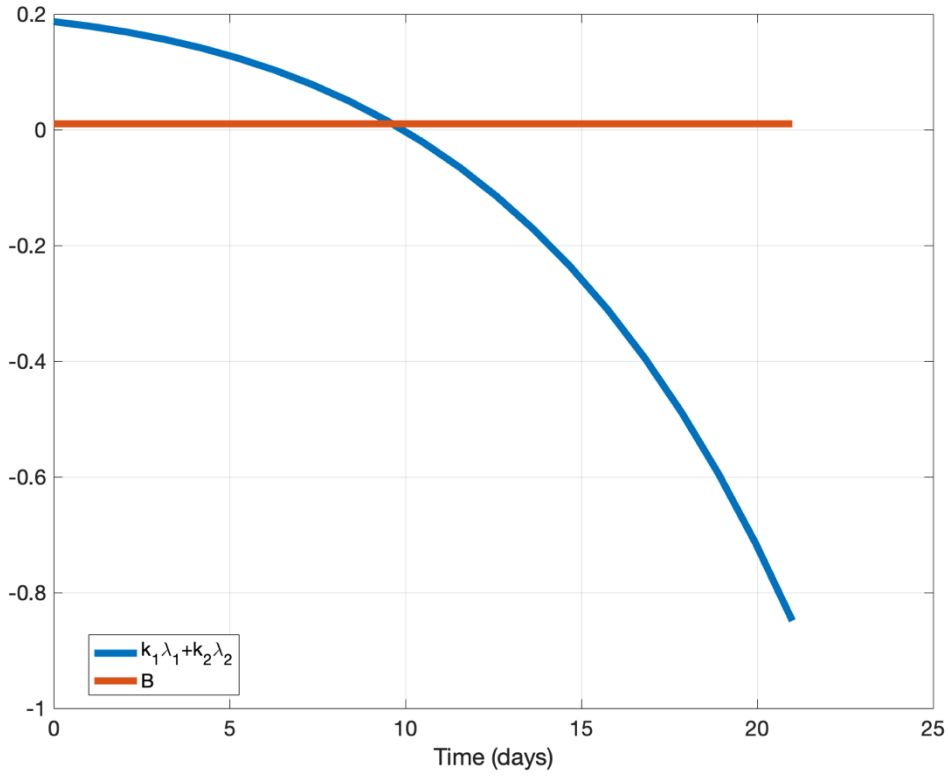


Figure 3-1 The method for determining $B$ utilizes the influence line. Taking a 21-day interval as an example $\mu = 11$ indicates that the TRIMP should be adjusted on day 10. By referring to the influence line, we identify $B$ as 0.01.

In addition to applying bang-bang control to generate a revised training program, we also construct an alternative regimen by calculating the average TRIMP within each interval and assigning this value uniformly across that interval. This approach allows us to examine whether redistributing the training load—rather than merely switching between extremes—can yield better performance on the final day.

To assess the effectiveness of these training strategies, all three methods—namely,



doi:10.6342/NTU202501357

the original optimal control-based program, the bang-bang control version, and the averaged TRIMP redistribution—are evaluated in terms of peak performance at the time of competition and total cumulative TRIMP over the entire training period.



doi:10.6342/NTU202501357

# Chapter 4 Results and Discussion

This section presents the simulation results and provides a comparative analysis among the different training strategies.

## 4.1 Baseline Simulation Outcomes without Optimal Control Application

Figures 4-1 through 4-8 present the simulation outcomes generated under training programs without the application of optimal control. These plots collectively depict the time evolution of performance, fitness, fatigue, and TRIMP throughout the training period, offering insights into their interdependencies and dynamic trends leading up to competition day. The simulations reveal that, during the initial stages of training, fatigue levels surpass those of fitness, resulting in a decline in performance. This pattern is likely due to the athlete's early physiological adaptation to training stimuli. When a persistently high TRIMP is applied, as illustrated in Figures 4-2 and 4-6, performance plateaus for an extended duration. This suggests that sustaining high-intensity training alone may not be an effective means to continually enhance performance, as it risks producing diminishing returns due to saturation effects.

In contrast, other training patterns involving reductions in TRIMP levels demonstrate noticeable performance gains. However, tapering too early—evident in Figures 4-3, 4-4, 4-7, and 4-8—fails to ensure peak performance on the competition day, which is the final day of training. These observations emphasize the importance of precisely timing load reductions to optimize final-day performance, underscoring the central objective of this



doi:10.6342/NTU202501357

study: to develop an optimized training regimen that guarantees peak performance at the desired time.

Table 1 provides a summary of competition-day performance and the total accumulated TRIMP for all simulation cases. The data suggest that, across different physiological profiles, consistently high training loads result in the lowest efficiency coefficients. This indicates that such an approach is suboptimal for maximizing performance. Conversely, programs that incorporate structured variation—such as tapering phases or symmetric load distributions—tend to produce superior performance outcomes relative to the total training load, as reflected by higher efficiency coefficients.

Moreover, athletes characterized by longer fitness retention times and faster fatigue recovery—such as those with parameters $(\eta_1, \eta_2) = (30,5)$—demonstrated higher overall efficiency across all evaluated training strategies. It is noteworthy that identical TRIMP distributions, $TR(t)$, can lead to varying performance outcomes depending on an athlete's physiological traits. For instance, under the parameter set $(\eta_1, \eta_2) = (25,10)$, the mid-cycle peak loading strategy produces the highest competition-day performance. Conversely, athletes with $(\eta_1, \eta_2) = (30,5)$ benefit more from the late tapering approach to reach peak performance.

Furthermore, while the symmetric loading pattern results in the greatest efficiency in both athlete profiles, the final-day performance under this strategy is the lowest for the $(30,5)$ a group but the second highest for the $(25,10)$ group. These results underscore the necessity of tailoring training regimens to individual physiological characteristics in order to optimize athletic outcomes.



doi:10.6342/NTU202501357

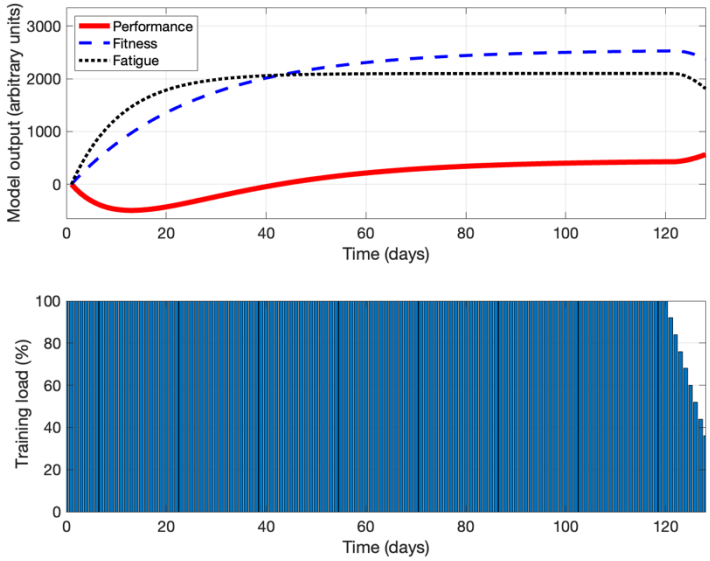


Figure 4-1 Modeling results for late tapering with parameters set as $(25, 10, 1, 2)$.

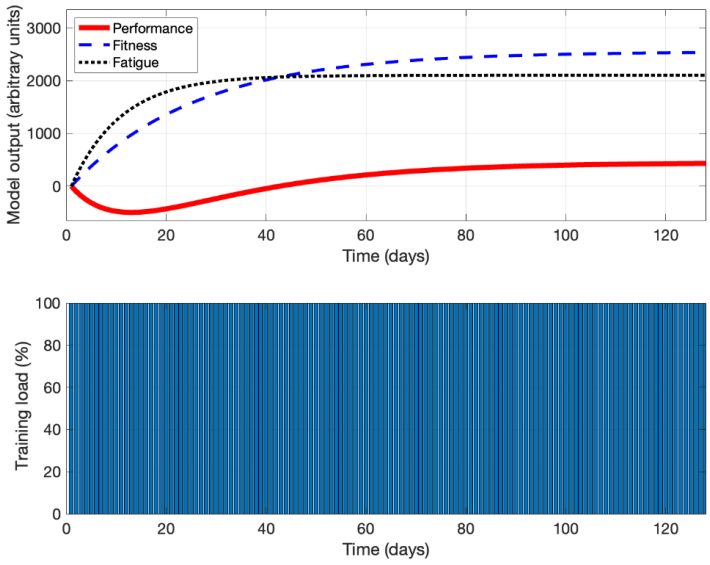


Figure 4-2 Modeling results for constant high load with parameters set as $(25, 10, 1, 2)$.



doi:10.6342/NTU202501357

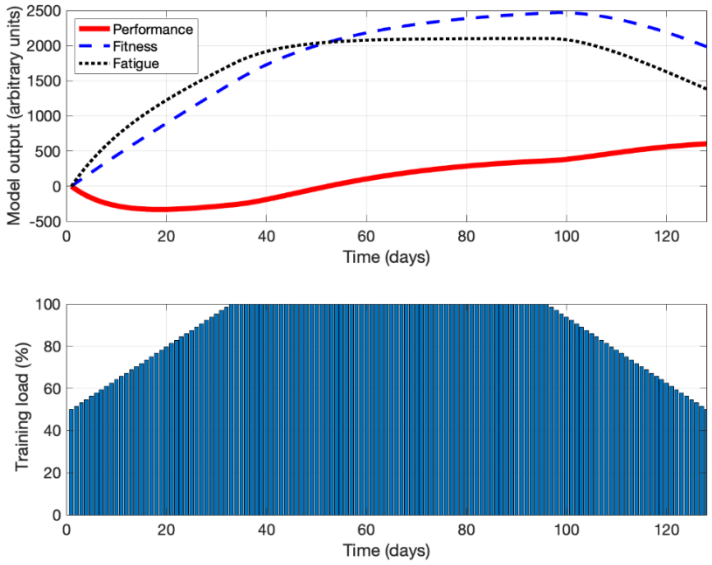


Figure 4-3 Modeling results for mid-cycle peak with parameters set as $(25, 10, 1, 2)$.

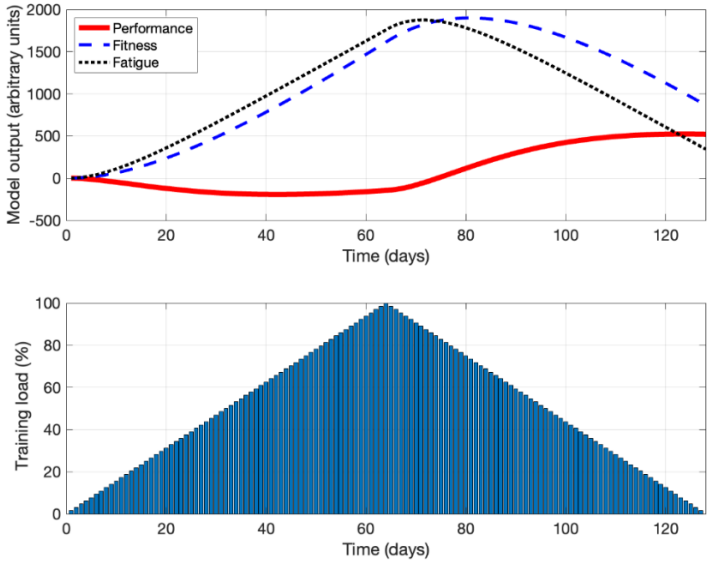


Figure 4-4 Modeling results for symmetric loading with parameters set as $(25, 10, 1, 2)$.



doi:10.6342/NTU202501357

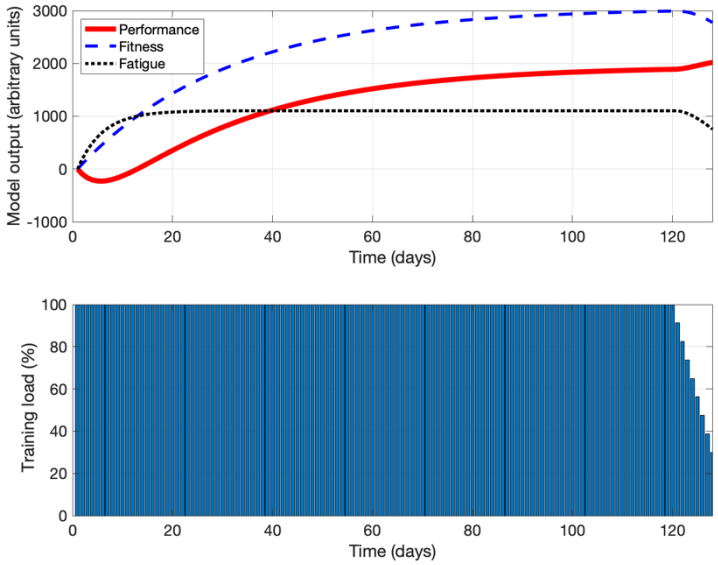


Figure 4-5 Modeling results for late tapering with parameters set as $(30, 5, 1, 2)$.

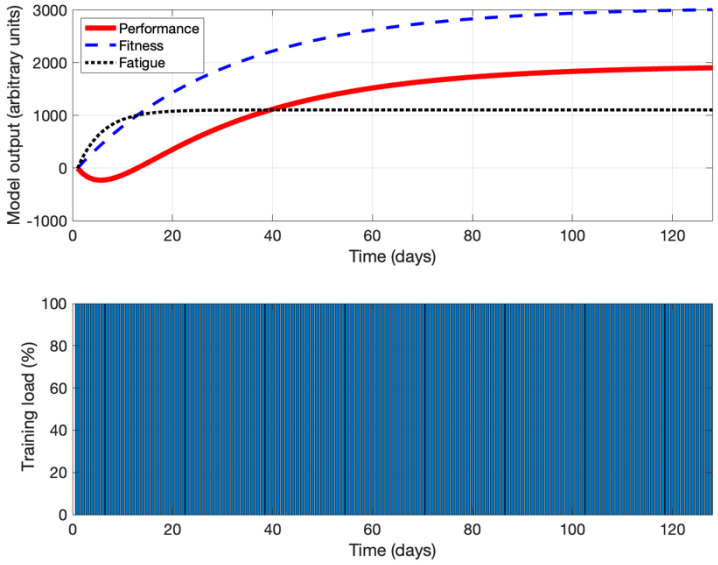


Figure 4-6 Modeling results for constant high load with parameters set as $(30, 5, 1, 2)$.



doi:10.6342/NTU202501357

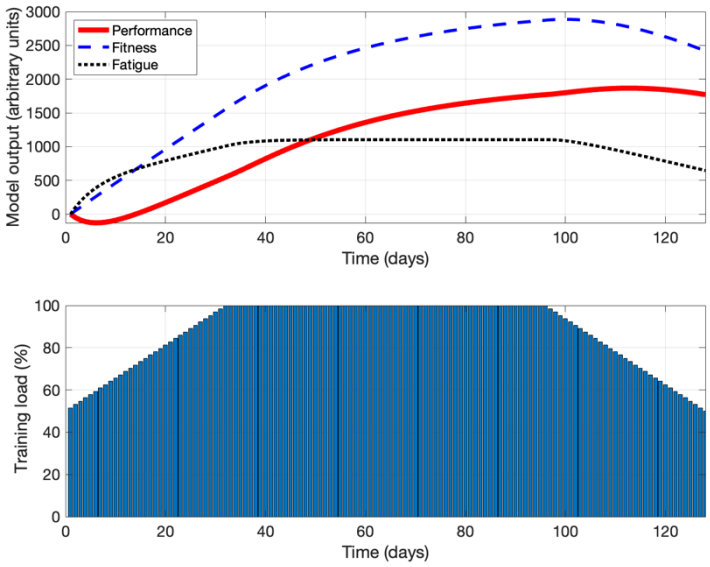


Figure 4-7 Modeling results for mid-cycle peak with parameters set as $(30, 5, 1, 2)$.

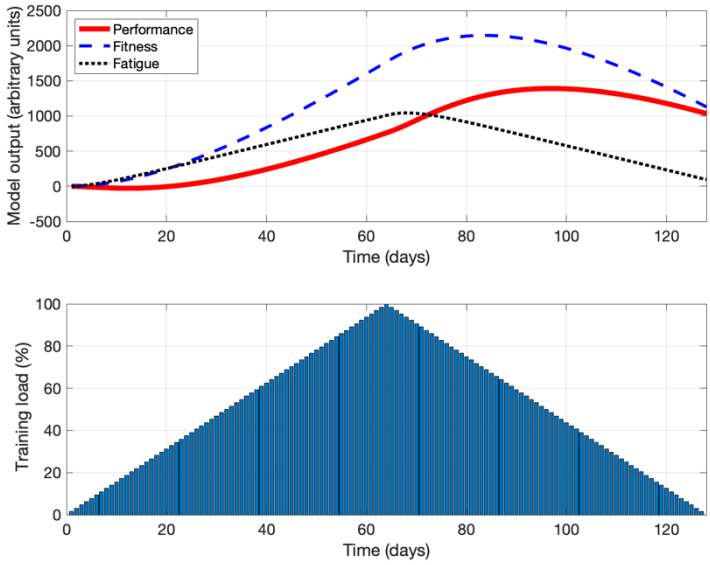


Figure 4-8 Modeling results for symmetric loading with parameters set as $(30, 5, 1, 2)$.



doi:10.6342/NTU202501357

Table 1**:** The values of $\alpha, \beta$ and efficiency coefficient (defined as the ratio of $\alpha$ to $\beta$) of every simulation experiment w/o OCT. $\alpha$: performance on competition day. $\beta$: cumulative TRIMP during training session. OCT: optimal control theory.

| $(\eta_1, \eta_2, k_1, k_2)$ | (25,10,1,2) | | | |
|---|---|---|---|---|
| $TR(t)$ type | late tapering | constant high load | mid-cycle peak | symmetric loading |
| $\alpha$ | 598 | 433 | 606 | 527 |
| $\beta$ | 12390 | 12800 | 11150 | 6500 |
| $\frac{\alpha}{\beta}$ | 0.0483 | 0.0340 | 0.0544 | 0.0811 |
| $(\eta_1, \eta_2, k_1, k_2)$ | (30,5,1,2) | | | |
| $TR(t)$ type | late tapering | constant high load | mid-cycle peak | symmetric loading |
| $\alpha$ | 2036 | 1904 | 1866 | 1392 |
| $\beta$ | 12390 | 12800 | 11150 | 6500 |
| $\frac{\alpha}{\beta}$ | 0.1643 | 0.1488 | 0.1666 | 0.2141 |

## 4.2 Simulation Outcomes Incorporating Optimal Control Theory

Figures 4-9 through 4-14 depict the simulation outcomes obtained via optimal control. It is evident that both fitness and fatigue increase concurrently with TRIMP.



doi:10.6342/NTU202501357

When TRIMP is maintained at its peak level, fitness continues to improve while fatigue reaches a plateau. Upon initiating the tapering phase, characterized by a reduction in TRIMP, both fitness and fatigue decrease accordingly. Importantly, performance rises during this period and ultimately attains its maximum on the final day, thereby fulfilling the objective of maximizing performance at competition time.

Comparisons between training regimens developed with and without the use of OCT reveal that strategically reducing TRIMP at the optimal time significantly enhances performance outcomes. For example, in non-optimized simulations, tapering through mid-cycle peak or symmetric loading patterns often occurs prematurely, leading to peak performance before the final day. Conversely, optimal control reliably aligns peak performance precisely with the competition day, removing the need for manual adjustment of taper timing and magnitude by coaches.

Moreover, Figures 4-9 and 4-12 illustrate that the optimal tapering onset varies substantially depending on individual physiological characteristics. While such variability must be explicitly accounted for in traditional program design, optimal control inherently integrates these factors. These findings underscore that effective training involves not merely increasing intensity or volume but rather balancing training stress and recovery in harmony with the athlete's unique physiological profile to optimize performance when it matters most.

Table 2 summarizes the competition-day performance and cumulative TRIMP across all simulations. Across different physiological profiles, simulations incorporating OCT consistently produce superior performance outcomes alongside reduced cumulative TRIMP relative to those without optimal control. This highlights the efficacy of our control framework in designing training plans that maximize peak



doi:10.6342/NTU202501357

performance while efficiently managing training load to reduce overtraining risk. Defining the efficiency coefficient as the ratio of competition-day performance to cumulative TRIMP, as shown in Table 2, further confirms these trends. The optimal control case with $TR(t)$ constrained between 0 and 100 achieves the highest efficiency, whereas simulations without optimal control exhibit the lowest. Within the optimal control scenarios, efficiency improves as the lower bound on $TR(t)$ is relaxed, indicating that allowing greater flexibility in training load enables more effective strategies to maximize performance while minimizing total TRIMP.

Overall, simulation results demonstrate that the optimal control approach yields higher competition-day performance compared to non-optimized programs. However, it is important to note that these findings are based on simulations of individual athletes, and the magnitude of performance improvement depends on specific physiological characteristics. For example, with parameters $(\eta_1, \eta_2, k_1, k_2) = (25,10,1,2)$, optimal control delivers a 44.82% improvement over the baseline, whereas for $(\eta_1, \eta_2, k_1, k_2) = (30,5,1,2)$, the gain is more modest at 2.16%. Despite such variability, even small improvements are significant in elite sports, where marginal gains can influence podium outcomes [51–53]. Prior research has shown that differences less than one or two percent often determine competition results [54, 55]. Therefore, the presented control framework remains valuable as it can confer meaningful competitive advantages, even with seemingly modest performance enhancements.



doi:10.6342/NTU202501357

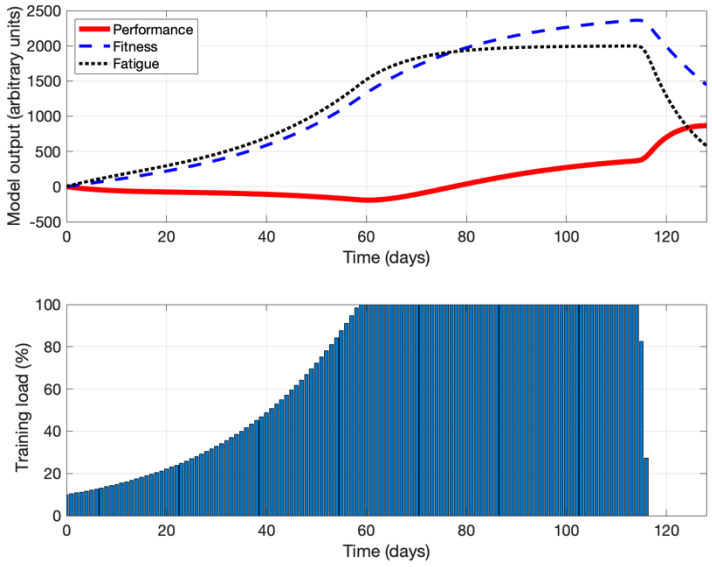


Figure 4-9 Modeling results by OCT with parameters set as $(25, 10, 1, 2)$ and $TR(t)$ between 0 and 100. OCT: optimal control theory.

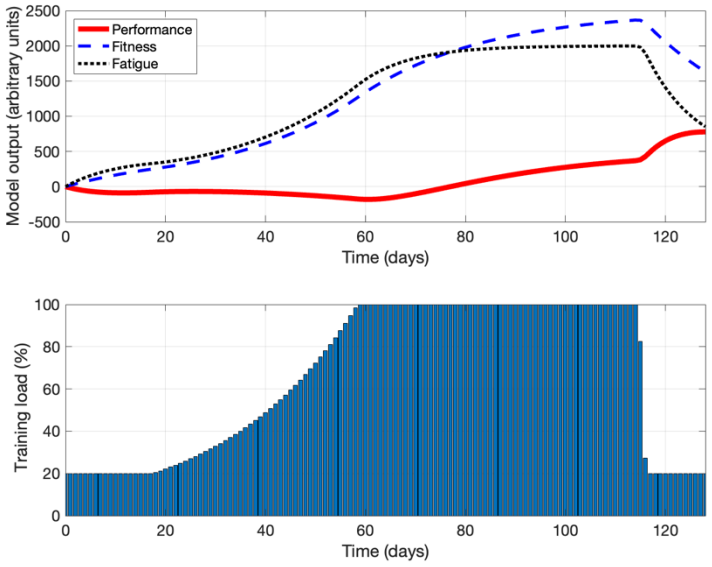


Figure 4-10 Modeling results by OCT with parameters set as $(25, 10, 1, 2)$ and $TR(t)$ between 20 and 100. OCT: optimal control theory.



doi:10.6342/NTU202501357

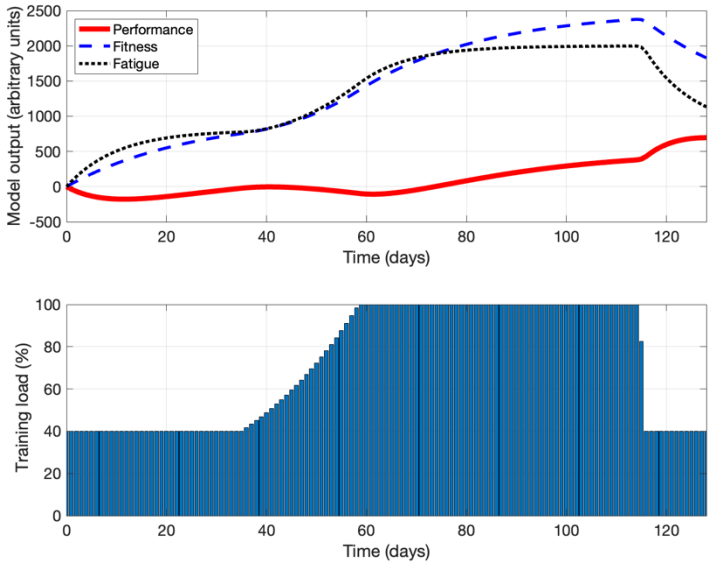


Figure 4-11 Modeling results by OCT with parameters set as $(25, 10, 1, 2)$ and $TR(t)$ between 40 and 100. OCT: optimal control theory.

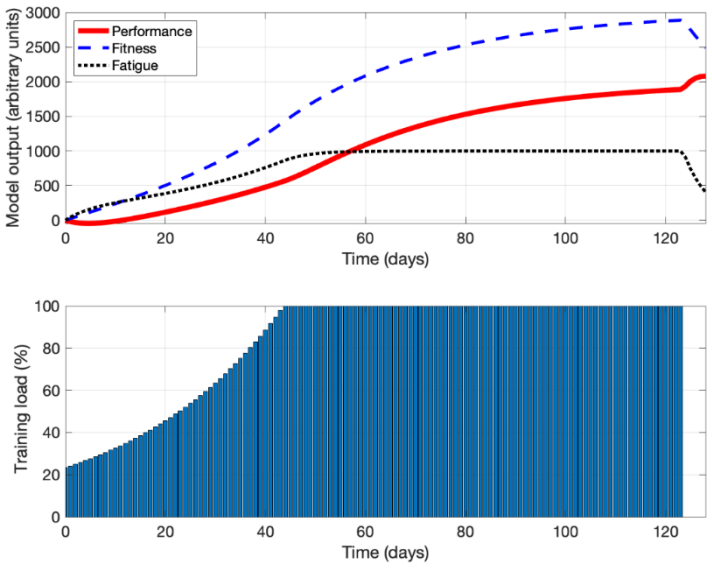


Figure 4-12 Modeling results by OCT with parameters set as $(30, 5, 1, 2)$ and $TR(t)$ between 0 and 100. OCT: optimal control theory.



doi:10.6342/NTU202501357

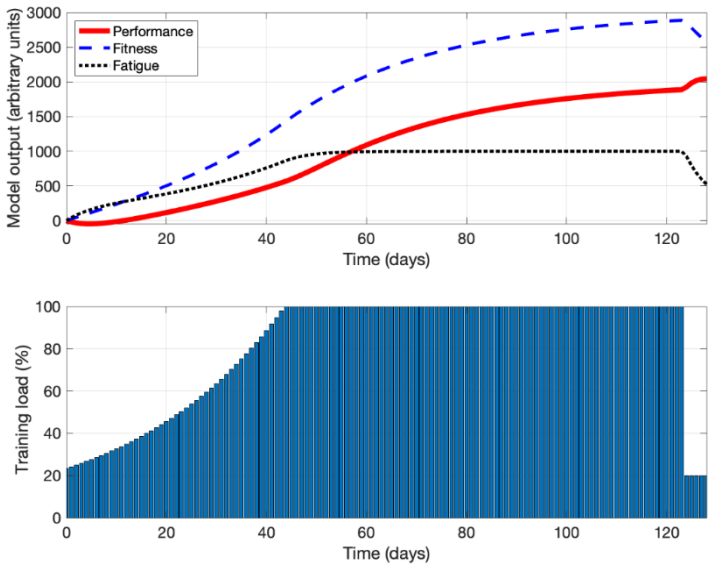


Figure 4-13 Modeling results by OCT with parameters set as $(30, 5, 1, 2)$ and $TR(t)$ between 20 and 100. OCT: optimal control theory.

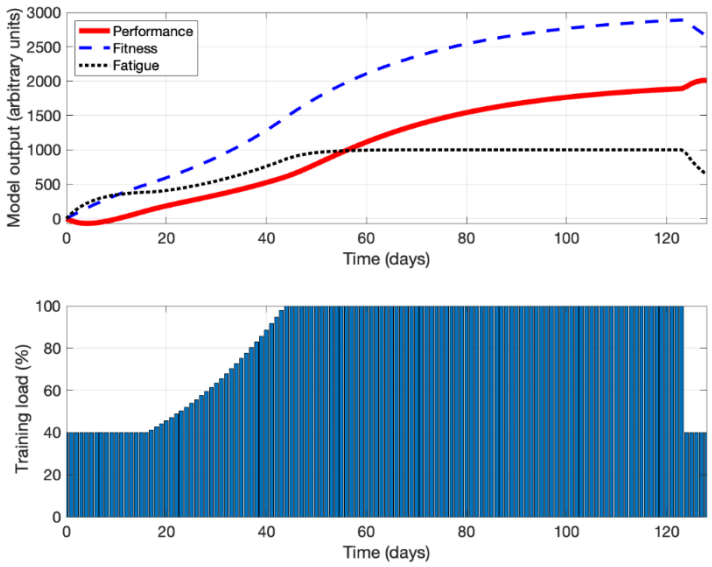


Figure 4-14 Modeling results by OCT with parameters set as $(30, 5, 1, 2)$ and $TR(t)$ between 40 and 100. OCT: optimal control theory.



doi:10.6342/NTU202501357

Table 2: The values of $\alpha, \beta$ and efficiency coefficient (defined as the ratio of $\alpha$ to $\beta$) of every simulation experiment with and w/o OCT. $\alpha$: performance on competition day. $\beta$: cumulative TRIMP during training session. OCT: optimal control theory.

| $(\eta_1, \eta_2, k_1, k_2) = (25,10,1,2)$ | w/ OCT | | | w/o OCT (tapering load) |
|---|---|---|---|---|
| $TR(t)$ range | $0 \le TR(t) \le 100$ | $20 \le TR(t) \le 100$ | $40 \le TR(t) \le 100$ | not applicable |
| $\alpha$ | 866 | 778 | 695 | 598 |
| $\beta$ | 8018 | 8362 | 9168 | 12390 |
| $\frac{\alpha}{\beta}$ | 0.1080 | 0.0930 | 0.0758 | 0.0483 |
| $(\eta_1, \eta_2, k_1, k_2) = (30,5,1,2)$ | w/ OCT | | | w/o OCT (tapering load) |
| $TR(t)$ range | $0 \le TR(t) \le 100$ | $20 \le TR(t) \le 100$ | $40 \le TR(t) \le 100$ | not applicable |
| $\alpha$ | 2080 | 2045 | 2013 | 2036 |
| $\beta$ | 10300 | 10400 | 10654 | 12390 |
| $\frac{\alpha}{\beta}$ | 0.2019 | 0.1966 | 0.1889 | 0.1643 |

## 4.3 Exploring the Role and Utility of Parameter $A$ in Control Optimization

This section explores the influence and practical significance of the parameter $A$ in Eq. (3.2.2). To better understand its role, consider the case where $A$ is set to 1 and the constraints on the optimal control function $TR(t)$ (hereafter denoted as $TR^*(t)$) are removed. Under such conditions, the behavior of $TR^*(t)$ becomes directly governed by



doi:10.6342/NTU202501357

Eq. (3.2.28), which is determined by the athlete's physiological characteristics $(\eta_1, \eta_2, k_1, k_2)$ as well as the value of *A* itself.

To illustrate this, we present simulation results for the physiological parameters $(\eta_1, \eta_2, k_1, k_2) = (25,10,1,2)$ , as shown in Figures 4-15 through 4-19. The results reveal that *A* significantly affects both the shape and the peak magnitude of the control function. In particular, a smaller value of $A$ yields a higher peak in $TR^*(t)$. For example, with $A = 1$ (Figure 4-15), the peak value of $TR^*(t)$ is approximately 0.1026, while Figures 4-16 and 4-17, corresponding to $A = 0.1$ and $A = 0.01$, respectively, show elevated peak values.

These findings confirm that $A$ acts as a scaling factor for the optimal TRIMP profile. Therefore, when applying our optimal control formulation—where $TR(t)$ bounded between 0 and 100—it becomes crucial to choose an appropriate *A* such that $TR^*(t)$ remains within feasible and practical limits. Moreover, $A$ also influences the number of days during which the athlete trains at maximum intensity.

For instance, if the training objective is to maximize final-day performance without regard to the total accumulated load, a smaller $A$ (e.g., 0.0001, as in Figure 4-18) may be used to push the system to its performance limit. On the other hand, if the goal is to balance peak performance with reduced cumulative TRIMP, a moderate $A$ value such as 0.001 (Figure 4-19) would be more suitable. Table 3 summarizes the outcomes for these two strategies. Although the scenario with $A = 0.001$ achieves superior competition-day performance, it also incurs a greater overall training burden. This comparison underscores the flexibility that $A$ provides, enabling coaches to tailor training plans to specific performance goals and load constraints. Regardless of the value chosen, both strategies based on our optimal control formulation consistently outperform non-



doi:10.6342/NTU202501357

optimized training approaches in terms of final-day performance and efficiency.

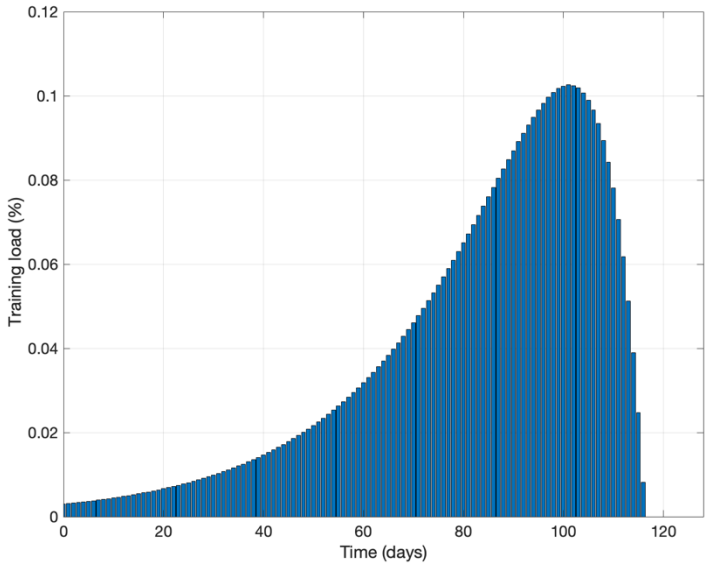


Figure 4-15 Optimal control $TR^*(t)$ for $A = 1$.

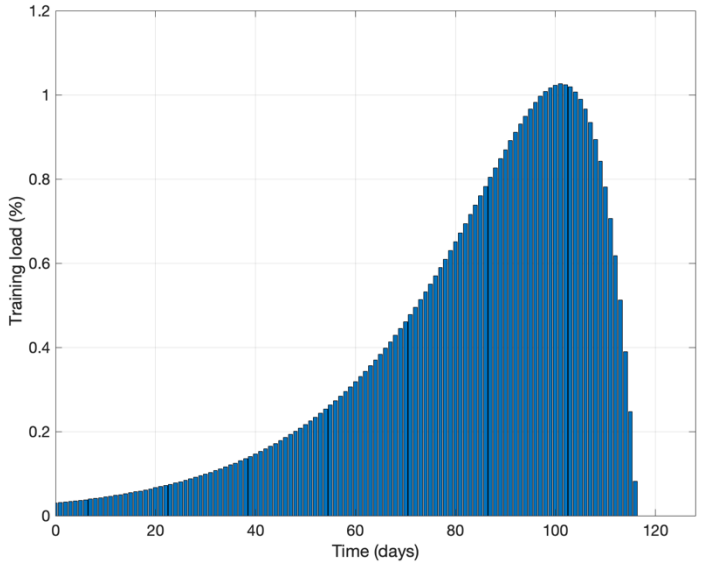


Figure 4-16 Optimal control $TR^*(t)$ for $A = 0.1$.



doi:10.6342/NTU202501357

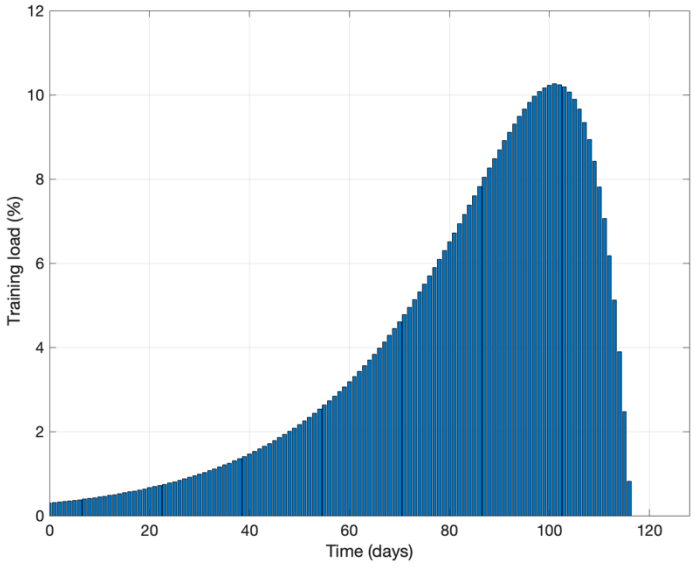


Figure 4-17 Optimal control $TR^*(t)$ for $A = 0.01$.

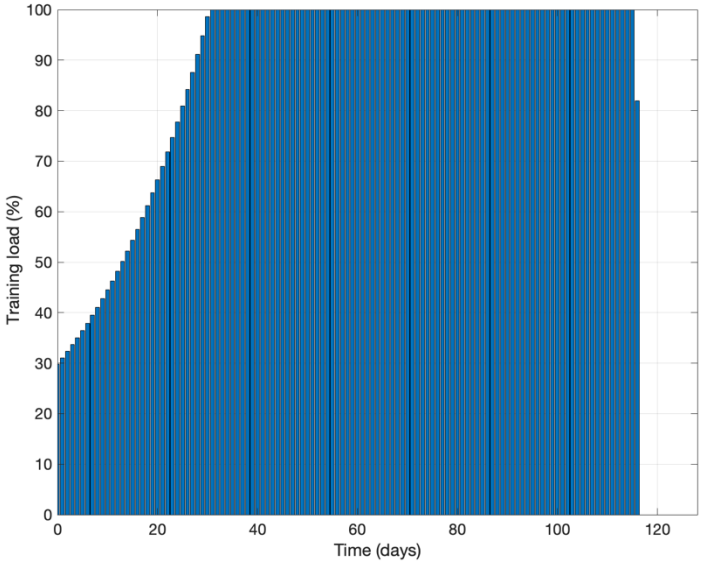


Figure 4-18 Optimal control $TR^*(t)$ for $A = 0.0001$.



doi:10.6342/NTU202501357

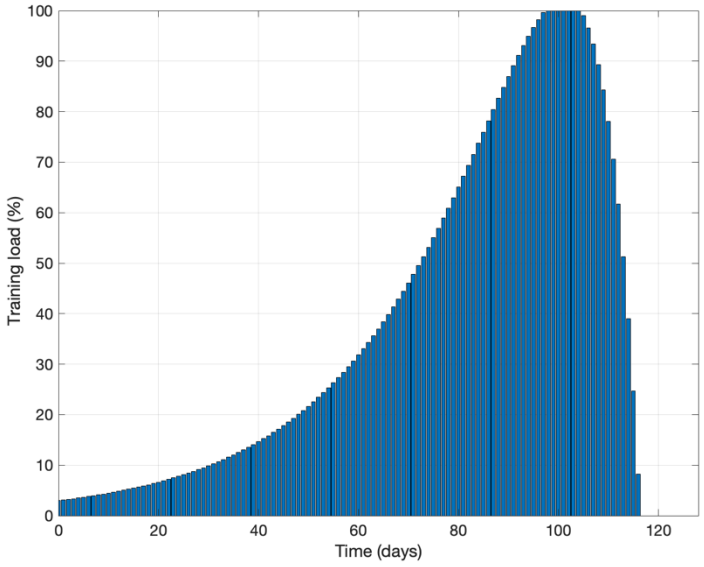


Figure 4-19 Optimal control $TR^*(t)$ for $A = 0.001$.

Table 3: The values of $\alpha$, $\beta$ and efficiency coefficient (defined as the ratio of $\alpha$ to $\beta$) of two simulations using OCT under $A = 0.0001$ and $0.001$ respectively ($TR(t)$ between 0 and 100). $\alpha$: performance on competition day. $\beta$: cumulative TRIMP during training session. OCT: optimal control theory.

| | w/ OCT | | w/o OCT (tapering load) |
|---|---|---|---|
| $A$ value | 0.0001 | 0.001 | not applicable |
| $\alpha$ | 917 | 635 | 598 |
| $\beta$ | 10374 | 4640 | 12390 |
| $\frac{\alpha}{\beta}$ | 0.0884 | 0.1368 | 0.0483 |



doi:10.6342/NTU202501357

## 4.4 Simulation Results Using Bang-Bang Control

The results of simulations conducted under OCT with TRIMP constrained between 0 and 100 are presented in Figure 4-20. These findings align with the trends observed in Section 4.2: both fitness and fatigue increase as TRIMP rises. However, since fatigue slightly outpaces fitness during this phase, performance exhibits a gradual decline. Once TRIMP reaches its peak, fatigue begins to decrease, allowing fitness to surpass it, which in turn drives a recovery in performance. As TRIMP continues to decline, performance improves markedly and ultimately peaks precisely on the competition day. Notably, TRIMP drops to zero on day 157, which coincides with the optimal tapering point suggested by the influence line. One of the key benefits of applying optimal control is that it automatically determines the ideal tapering schedule without requiring the explicit specification of the switching parameter $\mu$, thus ensuring maximal performance on the final day.

Figures 4-21 through 4-23 depict the simulation outcomes under bang-bang control with interval lengths of 14, 21, and 28 days, respectively. Comparing these results with Figure 4-20 provides insights into how different TRIMP adjustment schemes affect performance across the 168-day training period. The dynamics of performance, fitness, and fatigue under bang-bang control diverge substantially from those produced by optimal control. In the optimal control scenario, performance reaches a minimum of nearly -500 around day 100, followed by a steady rise culminating in peak performance on the final day. By contrast, bang-bang control generates localized performance peaks at the end of each training interval, offering a distinct practical advantage: if training is interrupted prematurely, athletes may still attain relatively high performance at these interim peaks. Minor fluctuations are observed across different interval lengths due to the



doi:10.6342/NTU202501357

design of bang-bang control, which inherently aims to produce periodic peaks, facilitating progress assessment and potential program adjustments.

A closer examination of Figures 4-21 to 4-23 reveals the influence of interval length on performance outcomes. Each training interval comprises a high TRIMP phase followed by a low TRIMP phase. Based on the influence line (Eq. 3.3.2), the low TRIMP phase is consistently maintained for the final 11 days of each interval, whereas the duration of the high TRIMP phase varies with interval length. Specifically, high TRIMP phases last 3, 10, and 17 days for the 14-day, 21-day, and 28-day intervals, respectively. These durations directly impact final-day performance. In Figure 4-21, where the high TRIMP phase spans only 3 days, the cumulative training load is insufficient, resulting in a lower final performance than that achieved under the optimal control program. In contrast, Figures 4-22 and 4-23, with longer high TRIMP durations of 10 and 17 days, show significantly improved final performance levels, surpassing even those attained via optimal control. Furthermore, under these longer intervals, performance remains non-negative throughout the training period, indicating more stable adaptation. These results imply that even if an athlete's training is unexpectedly interrupted, completing the current training cycle can still yield meaningful performance gains—particularly for programs using 21- or 28-day intervals—compared to both the shorter interval and the baseline optimal control design.

Table 4 summarizes the performance on the final day and the cumulative TRIMP across all simulation scenarios. The findings suggest that only the 21-day and 28-day interval programs outperform the optimal control scheme in terms of both peak performance and training efficiency. These results underscore that attaining high performance is not solely dependent on the total accumulated TRIMP, but also on maintaining an adequate duration of sustained high-load training within each interval.



doi:10.6342/NTU202501357

Among the evaluated programs, the 21-day interval emerges as the most balanced and effective configuration, offering a favorable trade-off between performance maximization and efficient training load management.

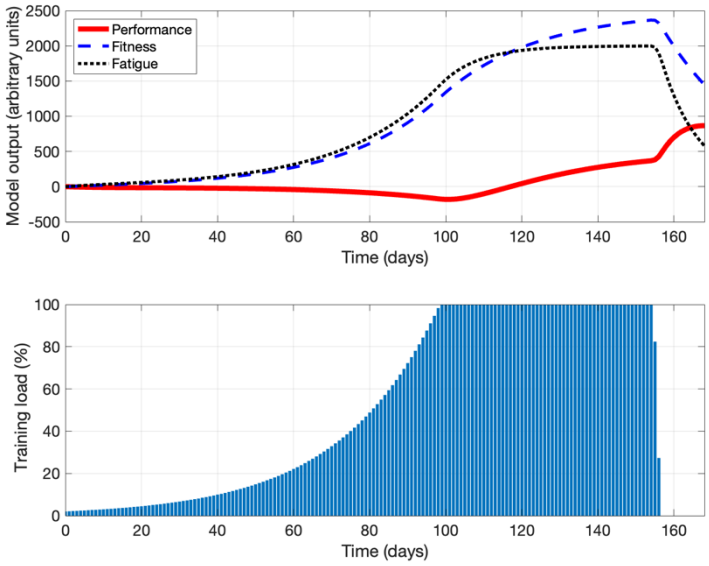


Figure 4-20 Modeling results by OCT and $TR(t)$ between 0 and 100. OCT: optimal control theory.



doi:10.6342/NTU202501357

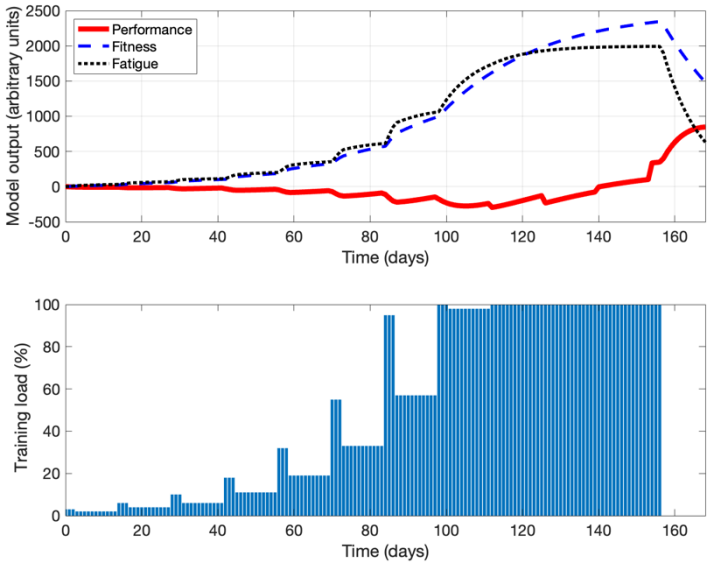


Figure 4-21 Modeling results for using bang-bang control with interval lengths of 14 days.

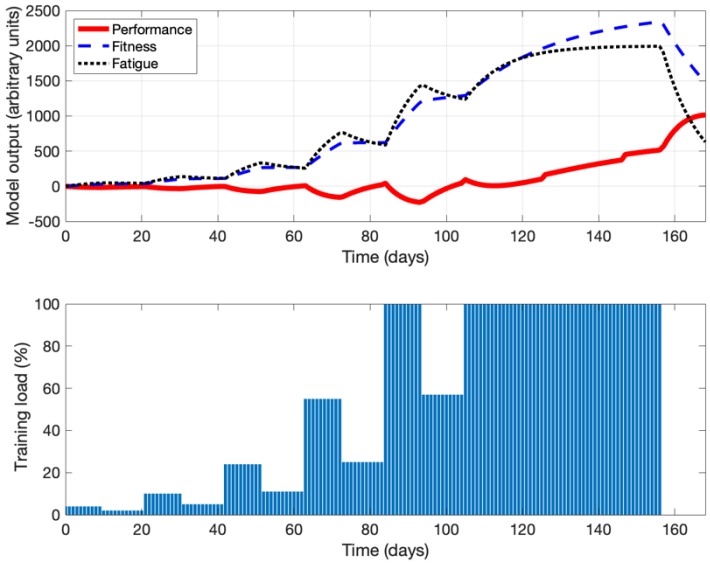


Figure 4-22 Modeling results for using bang-bang control with interval lengths of 21 days.



doi:10.6342/NTU202501357

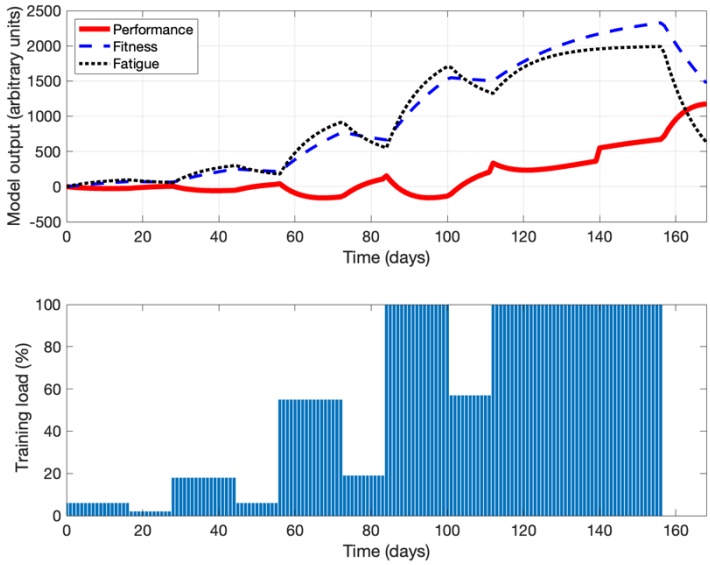


Figure 4-23 Modeling results for using bang-bang control with interval lengths of 28 days.

Table 4: The values of $\alpha, \beta$ and efficiency coefficient (defined as the ratio of $\alpha$ to $\beta$) of every simulation experiment with OCT and bang-bang control. $\alpha$: performance on competition day. $\beta$: cumulative TRIMP during training session. OCT: optimal control theory.

| | bang-bang control | | | OCT |
|---|---|---|---|---|
| Interval length (days) | 14 | 21 | 28 | not applicable |
| $\alpha$ | 848 | 1016 | 1175 | 866 |
| $\beta$ | 7981 | 8226 | 8463 | 8213 |
| $\frac{\alpha}{\beta}$ | 0.1062 | 0.1235 | 0.1388 | 0.1055 |



doi:10.6342/NTU202501357

## 4.5 Simulation Results Using Average Method

In addition to implementing bang-bang control to simplify the optimal TRIMP profile, we explored an alternative method in which the average TRIMP value within each interval is assigned uniformly across all days in that interval. Simulation results corresponding to this approach are presented in Figures 4-24 through 4-26. Although this averaging strategy streamlines daily training loads and bears similarities to the bang-bang control pattern, the overall trajectories of fitness, fatigue, and performance closely mirror those generated by the original optimal control strategy. However, in simulations using 21-day and 28-day intervals, the final-day performance fails to reach its maximum potential. This is primarily due to the fact that TRIMP values in the last interval are not reduced to zero, thereby depriving athletes of sufficient recovery time. Consequently, peak performance cannot be realized on the competition day.

Table 5 provides a summary of competition-day performance and cumulative TRIMP for all trials. The results indicate that the averaging approach underperforms in both peak performance and efficiency when compared with the optimal control strategy. These findings suggest that simply smoothing TRIMP via interval averages does not adequately address the physiological demands of training adaptation and fatigue management.

To mitigate this issue, we propose a refined strategy where the TRIMP value in the final interval directly follows the trajectory defined by the optimal control solution. This modification is designed to provide adequate rest in the lead-up to competition and improve performance on the final day.



doi:10.6342/NTU202501357

Figures 4-27 to 4-29 present the results from this hybrid approach, and the corresponding performance and cumulative TRIMP data are summarized in Table 6. Although the general trends remain similar to those in the earlier averaging method, the inclusion of the optimized tapering phase ensures that the final-day performance reaches its peak. Despite this improvement, both overall efficiency and peak performance still fall short of those attained through the full optimal control framework. This outcome suggests that while the averaging approach may enhance the practicality of implementation, its effectiveness in boosting performance remains limited. By contrast, the bang-bang control method not only achieves higher peak performance but also improves efficiency, making it a more robust choice for practical training modifications.

Among all six simulations, the 14-day interval under the average TRIMP method produces the highest final-day performance and efficiency. On the other hand, the 28-day interval under bang-bang control yields the best outcomes in both metrics. This pattern may be attributed to the switching point in bang-bang control, which typically occurs around day 17, resulting in two training phases of approximately 17 and 11 days—durations closely aligned with those observed in the averaging method.

These findings underscore the importance of appropriately timing TRIMP adjustments to balance physiological adaptation and recovery. Training programs with excessively frequent or entirely absent TRIMP changes tend to be less effective. Based on these results, maintaining a consistent TRIMP level for approximately 11 to 17 days appears to offer the most favorable outcomes in terms of both performance and training efficiency.



doi:10.6342/NTU202501357

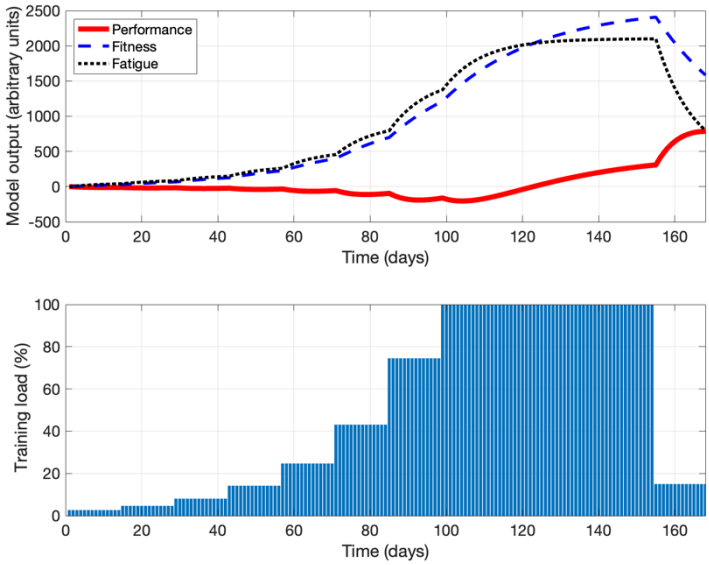


Figure 4-24 Modeling results for using average TRIMP with interval lengths of 14 days.

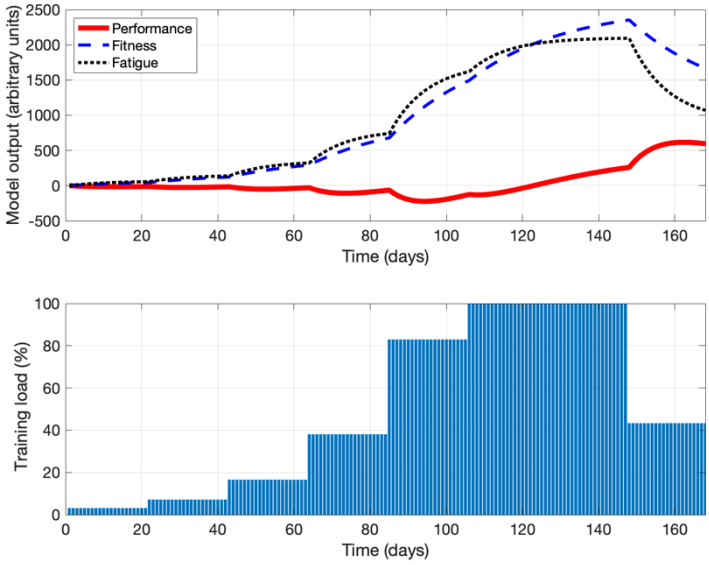


Figure 4-25 Modeling results for using average TRIMP with interval lengths of 21 days.



doi:10.6342/NTU202501357

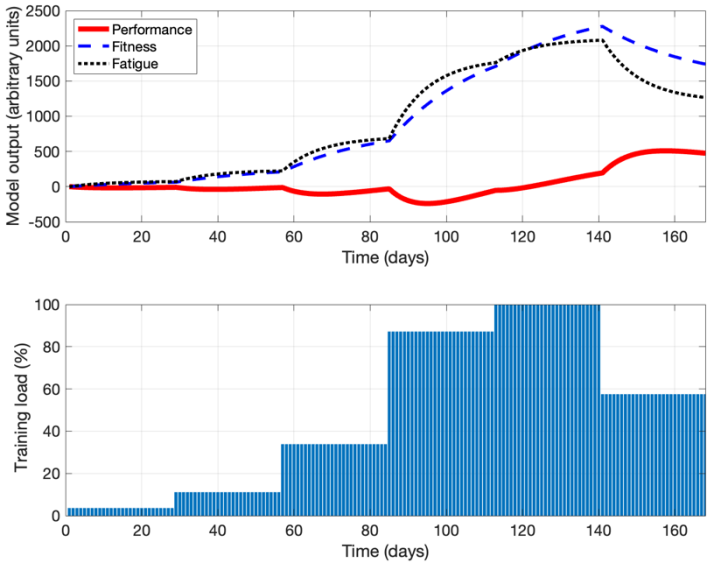


Figure 4-26 Modeling results for using average TRIMP with interval lengths of 28 days.

Table 5: The values of $\alpha, \beta$ and efficiency coefficient (defined as the ratio of $\alpha$ to $\beta$) of every simulation experiment with OCT and average TRIMP. $\alpha$: performance on competition day. $\beta$: cumulative TRIMP during training session OCT: optimal control theory.

| | OCT with average TRIMP | | | OCT |
|---|---|---|---|---|
| Interval length (days) | 14 | 21 | 28 | not applicable |
| $\alpha$ | 785 | 616 | 509 | 866 |
| $\beta$ | 8213 | 8213 | 8213 | 8213 |
| $\frac{\alpha}{\beta}$ | 0.0956 | 0.075 | 0.062 | 0.1055 |



doi:10.6342/NTU202501357

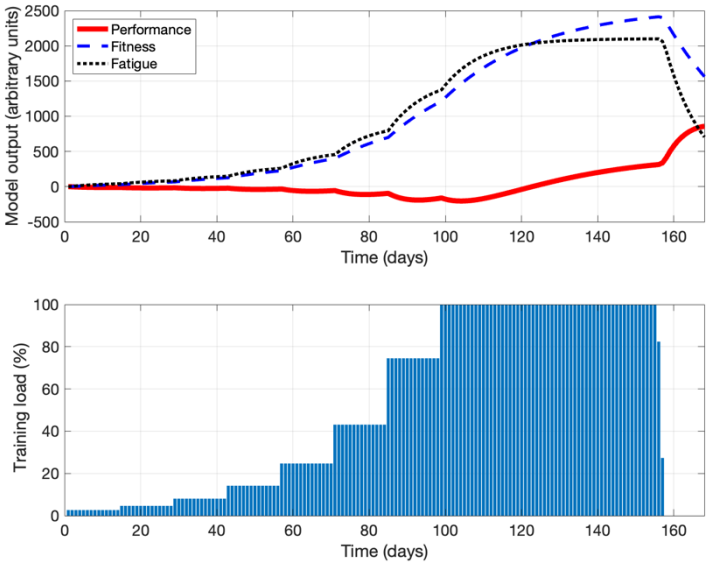


Figure 4-27 Modeling results for using average TRIMP (final interval following OCT behavior) with interval lengths of 14 days.

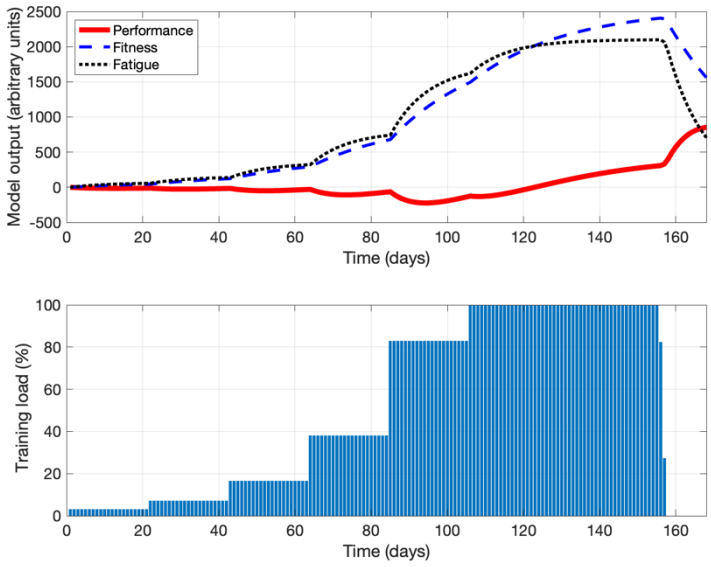


Figure 4-28 Modeling results for using average TRIMP (final interval following OCT behavior) with interval lengths of 21 days.



doi:10.6342/NTU202501357

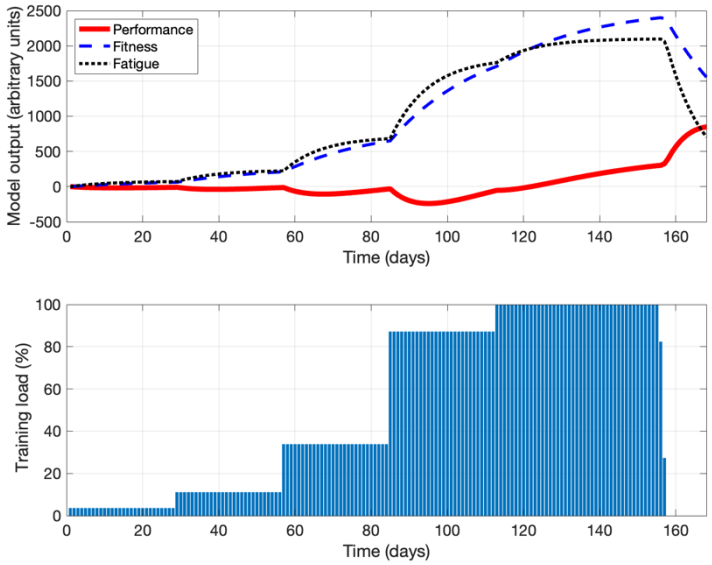


Figure 4-29 Modeling results for using average TRIMP (final interval following OCT behavior) with interval lengths of 28 days.

Table 6: The values of $\alpha, \beta$ and the efficiency coefficient (defined as the ratio of $\alpha$ to $\beta$) of every simulation experiment with OCT and average TRIMP but final interval following OCT behavior. $\alpha$: performance on competition day. $\beta$: the cumulative TRIMP during training session. OCT: optimal control theory.

| | OCT with average TRIMP and final interval set to follow OCT behavior | | | OCT |
|---|---|---|---|---|
| Interval length (days) | 14 | 21 | 28 | not applicable |
| $\alpha$ | 864 | 860 | 856 | 866 |
| $\beta$ | 8213 | 8213 | 8213 | 8213 |
| $\frac{\alpha}{\beta}$ | 0.1051 | 0.1047 | 0.1042 | 0.1055 |



doi:10.6342/NTU202501357

## 4.6 Discussion of Present Study Limitations

It is important to recognize the limitations inherent in this study. First, the performance model adopted herein is empirical or phenomenological in nature—constructed based on observed trends and conceptual insights rather than grounded in mechanistic physiological principles. As such, it captures only the aggregate impact of training, namely the dual effects of fitness and fatigue on performance, while neglecting the distinct contributions of specific physiological or psychological components.

Second, the model characterizes the dynamics of fitness and fatigue through first-order linear differential equations. Although this approach offers mathematical simplicity and ease of interpretation, it may fail to adequately reflect the inherently nonlinear and complex interactions between training stimuli and performance outcomes. To overcome this limitation, numerous extensions of the original Banister IR model have been suggested, incorporating more advanced mathematical structures to enhance descriptive and predictive capabilities [23, 26, 29, 30, 56–58].

Third, the current framework assumes the athlete-specific parameters—namely $\eta_1$, $\eta_2$, $k_1$ and $k_2$ in Eq. (3.1.11) —remain constant over time. In practice, however, an athlete's physiological responsiveness evolves throughout the training process. Therefore, a more realistic formulation would allow these parameters to vary with time, reflecting ongoing adaptations to training stimuli [1, 4, 59].

In summary, this pilot study utilized a simplified training-performance model to integrate OCT into the construction of training regimens. The simplicity of the model was a deliberate design choice, aimed at enabling clear analytical development and manageable computational implementation. This allowed us to show the feasibility of the proposed framework and to establish the existence and uniqueness of optimal solutions.



doi:10.6342/NTU202501357

Future work should consider employing more sophisticated and physiologically grounded models to better capture the nuances of training adaptation. In addition, empirical validation will be essential to determine whether the proposed control-based approach can effectively guide training design, not only to optimize performance on competition day but also to regulate training load and mitigate the risk of overtraining.



doi:10.6342/NTU202501357

# Chapter 5 Conclusion

This study introduces a novel application of OCT to the design of personalized sports training programs—a direction that, to the best of our knowledge, has not been thoroughly explored in previous literature. The proposed approach offers coaches, trainers, and athletes a systematic framework for planning individualized training schedules that align with each athlete's unique physiological profile.

Our simulation results demonstrate that applying an identical TRIMP distribution to different athletes leads to divergent performance outcomes on the competition day. Even for a single athlete, alternative training schedules can produce varying final performances. By incorporating OCT, training plans can be automatically optimized to minimize cumulative TRIMP while maximizing performance at the target date, with individual physiological parameters explicitly considered. This control-based methodology provides a valuable tool for managing training load throughout the preparation period and guiding athletes toward achieving peak performance while mitigating the risk of overtraining.

Additionally, this study explores two practical adaptations of the optimal training plan. The averaging method simplifies implementation by replacing daily TRIMP values with interval-based averages. Although this adjustment enhances real-world feasibility, its performance efficiency remains similar to that of the original optimal control approach. In contrast, the bang-bang control strategy not only facilitates practical execution but also enhances both peak performance and training efficiency. Notably, findings suggest that maintaining a constant TRIMP level for approximately 11 to 17 consecutive days yields the most favorable outcomes. Intervals shorter than this may fail to sustain performance improvements.



doi:10.6342/NTU202501357

It is important to acknowledge that all conclusions in this study are derived from numerical simulations. Future investigations should incorporate empirical validation using real-world athlete data to assess the model's predictive capability and practical impact. Moreover, as noted in the discussion of limitations, the current framework employs a simplified linear model that does not capture all dimensions of athletic adaptation. Specifically, it assumes constant values for the parameters $\eta_1$, $\eta_2$, $k_1$ and $k_2$ resulting in a fixed fatigue accumulation rate even during prolonged periods of high TRIMP. In practice, fatigue may escalate nonlinearly under sustained high-intensity training. Thus, integrating more advanced modeling approaches—such as the nonlinear models proposed by Turner et al. [29]—would more accurately reflect physiological realities.

In summary, this work demonstrates the viability and potential of OCT as a decision-support tool in sports science, particularly in crafting individualized training strategies. It establishes a foundation for future studies combining optimal control methods with more physiologically realistic models, paving the way for data-driven, performance-oriented training design that enhances competitive readiness while safeguarding athlete health.



doi:10.6342/NTU202501357

# REFERENCES


1. Borresen, J., & Lambert, M. I. (2009). The quantification of training load, the training response and the effect on performance. *Sports Medicine*, 39(9), 779–795.
2. Durell, D. L., Pujol, T. J., & Barnes, J. T. (2003). A survey of the scientific data and training methods utilized by collegiate strength and conditioning coaches. *The Journal of Strength & Conditioning Research*, 17(2), 368–373.
3. Clarke, D. C., & Skiba, P. F. (2013). Rationale and resources for teaching the mathematical modeling of athletic training and performance. *Advances in Physiology Education*, 37(2), 134-152.
4. Taylor, R. E., Zheng, C., Jackson, R. P., Doll, J. C., Chen, J. C., Holzbaur, K. R. S., ... & Kuhl, E. (2009). The phenomenon of twisted growth: humeral torsion in dominant arms of high performance tennis players. *Computer Methods in Biomechanics and Biomedical Engineering*, 12(1), 83-93.
5. Seth, A., Dong, M., Matias, R., & Delp, S. (2019). Muscle contributions to upper-extremity movement and work from a musculoskeletal model of the human shoulder. *Frontiers in Neurorobotics*, 13, 90.
6. Kirk, D. E. (2012). Optimal control theory: An introduction. *Courier Corporation*.
7. Hull, D. G. (2013). Optimal control theory for applications. S*pringer Science & Business Media.*
8. Macki, J., & Strauss, A. (2012). Introduction to optimal control theory. *Springer Science & Business Media.*
9. Ma, Z., & Zou, S. (2021). Optimal control theory. *Springer.*
10. Prestes, J., De Lima, C., Frollini, A. B., Donatto, F. F., & Conte, M. (2009). Comparison of linear and reverse linear periodization effects on maximal strength




doi:10.6342/NTU202501357

and body composition. *The Journal of Strength & Conditioning Research*, 23(1), 266–274.

11. Issurin, V. (2008). Block periodization versus traditional training theory: A review. *Journal of Sports Medicine and Physical Fitness*, 48(1), 65–75.
12. Painter, K. B., Haff, G. G., Ramsey, M. W., McBride, J., Triplett, T., Sands, W. A., ... & Stone, M. H. (2012). Strength gains: Block versus daily undulating periodization weight training among track and field athletes. *International Journal of Sports Physiology and Performance*, 7(2), 161–169.
13. Dave, A. G., & Elite, R. (2013). Sport Performance Division.
14. Hawkins, M. N., Raven, P. B., Snell, P. G., Stray-Gundersen, J., & Levine, B. D. (2007). Maximal oxygen uptake as a parametric measure of cardiorespiratory capacity. *Medicine & Science in Sports & Exercise*, 39(1), 103–107.
15. Abut, F., Akay, M. F., & George, J. (2016). Developing new VO2max prediction models from maximal, submaximal and questionnaire variables using support vector machines combined with feature selection. *Computers in Biology and Medicine*, 79, 182–192.
16. Koutlianos, N., Dimitros, E., Metaxas, T., Cansiz, M., Deligiannis, A. S., & Kouidi, E. (2013). Indirect estimation of VO2max in athletes by ACSM's equation: Valid or not? *Hippokratia*, 17(2), 136–140.
17. Akay, M. F., Shokrollahi, N., Aktürk, E., & George, J. D. (2011). Development of new VO2max prediction models by using artificial neural networks. *In Kusadasi, Turkey: Intl. Symp. on Computing in Science and Engineering* (pp. 39-44).



doi:10.6342/NTU202501357

18. Abut, F., & Akay, M. F. (2015). Machine learning and statistical methods for the prediction of maximal oxygen uptake: Recent advances. *Medical Devices: Evidence and Research*, 8, 369–379.
19. Akay, M. F., Inan, C., Bradshaw, D. I., & George, J. D. (2009). Support vector regression and multilayer feed forward neural networks for non-exercise prediction of VO2max. *Expert Systems with Applications*, 36(6), 10112–10119.
20. Banister, E. W., Calvert, T. W., Savage, M. V., & Bach, T. (1975). A systems model of training for athletic performance. *Australian Journal of Sports Medicine*, 7(3), 57–61.
21. Calvert, T. W., Banister, E. W., Savage, M. V., & Bach, T. (1976). A systems model of the effects of training on physical performance. *IEEE Transactions on Systems, Man, and Cybernetics*, SMC-6(2), 94–102.
22. Perl, J. (2001). PerPot: A metamodel for simulation of load performance interaction. *European Journal of Sport Science*, 1(2), 1–13.
23. Busso, T. (2003). Variable dose-response relationship between exercise training and performance. *Medicine & Science in Sports & Exercise*, 35(7), 1188–1195.
24. Morton, R. H., Fitz-Clarke, J. R., & Banister, E. W. (1990). Modeling human performance in running. *Journal of Applied Physiology*, 69(3), 1171–1177.
25. Bannister, E. (1991). Modeling elite athletic performance. In Physiological Testing of the High–Performance Athlete (Ed. J. MacDougall, H. Wenger, H. Green).
26. Hellard, P., Avalos, M., Lacoste, L., Barale, F., Chatard, J. C., & Millet, G. P. (2006). Assessing the limitations of the Banister model in monitoring training. *Journal of Sports Sciences*, 24(5), 509–520.



doi:10.6342/NTU202501357

27. Taha, T., & Thomas, S. G. (2003). Systems modelling of the relationship between training and performance. *Sports Medicine*, 33, 1061–1073.
28. Pfeiffer, M. (2008). Modeling the relationship between training and performance: A comparison of two antagonistic concepts. *International Journal of Computer Science in Sport*, 7(2), 13–32.
29. Turner, J. D., Mazzoleni, M. J., Little, J. A., Sequeira, D., & Mann, B. P. (2017). A nonlinear model for the characterization and optimization of athletic training and performance. *Biomedical Human Kinetics*, 9(1), 82–93.
30. Peng, K., Brodie, R. T., Swartz, T. B., & Clarke, D. C. (2024). Bayesian inference of the impulse-response model of athlete training and performance. I*nternational Journal of Performance Analysis in Sport*, 24(1), 74–89.
31. Luteberget, L. S., Houtmeyers, K. C., Vanrenterghem, J., Jaspers, A., Brink, M. S., & Helsen, W. F. (2021). Load monitoring practice in elite women association football. *Frontiers in Sports and Active Living*, 3, 715122.
32. Lamberti, N., Piva, G., Businaro, F., Caruso, L., Crepaldi, A., López-Soto, P. J., & Manfredini, F. (2022). A fitness-fatigue model of performance in peripheral artery disease: Predicted and measured effects of a pain-free exercise program. *Journal of Personalized Medicine*, 12(3), 397.
33. Mandorino, M., Gabbett, T. J., Tessitore, A., Leduc, C., Persichetti, V., & Lacome, M. (2025). The Interaction of Fitness and Fatigue on Physical and Tactical Performance in Football. *Applied Sciences*, 15(7), 3574.
34. Jeffries, A. C., Marcora, S. M., Coutts, A. J., Wallace, L., McCall, A., & Impellizzeri, F. M. (2022). Development of a revised conceptual framework of physical training for use in research and practice. *Sports Medicine*, 1-16



doi:10.6342/NTU202501357

35. Borrani, F., Solsona, R., Candau, R., Méline, T., & Sanchez, A. M. (2021). Modelling performance with exponential functions in elite short-track speed skaters. *Journal of Sports Sciences,* 39(20), 2378-2385.
36. Luenberger, D. G. (1979). Introduction to dynamic systems: Theory, models, and applications. *John Wiley & Sons.*
37. Kamien, M. I., & Schwartz, N. L. (2012). Dynamic optimization: The calculus of variations and optimal control in economics and management. *Courier Corporation.*
38. Lenhart, S., & Workman, J. T. (2007). Optimal control applied to biological models. *Chapman and Hall/CRC.*
39. Marchal, A., Benazieb, O., Weldegebriel, Y., Méline, T., & Imbach, F. (2025). Statistical flaws of the fitness-fatigue sports performance prediction model. *Scientific Reports,* 15(1), 3706.
40. Royden, H. L. (1968). Real analysis. Macmillan *Publishing Co*.
41. Rudin, W. (1987). Real and complex analysis. *McGraw-Hill.*
42. Stein, E. M., & Shakarchi, R. (2009). Real analysis: Measure theory, integration, and Hilbert spaces. *Princeton University Press*.
43. Pontryagin, L. S. (2018). Mathematical theory of optimal processes. Routledge.
44. Mason, L., Connolly, J., Devenney, L. E., Lacey, K., O'Donovan, J., & Doherty, R. (2023). Sleep, nutrition, and injury risk in adolescent athletes: A narrative review. *Nutrients*, 15(24), 5101.
45. Nobari, H., Cholewa, J. M., & Suzuki, K. (2023). Sports immunometabolism, training load, and nutrition: Effects on sports performance and psychological behavior of athletes. *Frontiers in Psychology*, 14, 1253502.



doi:10.6342/NTU202501357

46. Vermeire, K. M., Van de Casteele, F., Gosseries, M., Bourgois, J. G., Ghijs, M., & Boone, J. (2021). The influence of different training load quantification methods on the fitness-fatigue model. *International Journal of Sports Physiology and Performance*, 16(9), 1261–1269.
47. Butcher, J. C. (1966). On the convergence of numerical solutions to ordinary differential equations. *Mathematics of Computation*, 20(93), 1–10.
48. Butcher, J. C. (1967). A multistep generalization of Runge-Kutta methods with four or five stages. *Journal of the ACM*, 14(1), 84–99.
49. Fitz-Clarke, J. R., Morton, R. H., & Banister, E. W. (1991). Optimizing athletic performance by influence curves. *Journal of Applied Physiology*, 71(3), 1151–1158.
50. Pyne, D. B., Hopkins, W. G., Batterham, A. M., Gleeson, M., & Fricker, P. A. (2005). Characterising the individual performance responses to mild illness in international swimmers. *British Journal of Sports Medicine*, 39(10), 752–756
51. Bradshaw, E. J., Hume, P. A., & Aisbett, B. (2012). Performance score variation between days at Australian national and Olympic women's artistic gymnastics competition. *Journal of Sports Sciences*, 30(2), 191–199.
52. Lim, J. J., & Kong, P. W. (2013). Effects of isometric and dynamic postactivation potentiation protocols on maximal sprint performance. *The Journal of Strength & Conditioning Research*, 27(10), 2730–2736.
53. Park, J. L., Fairweather, M. M., & Donaldson, D. I. (2015). Making the case for mobile cognition: EEG and sports performance. *Neuroscience & Biobehavioral Reviews*, 52, 117–130.
54. Currell, K., & Jeukendrup, A. E. (2008). Validity, reliability and sensitivity of measures of sporting performance. *Sports Medicine*, 38, 297–316.



doi:10.6342/NTU202501357

55. Bellar, D., LeBlanc, N. R., & Campbell, B. (2015). The effect of 6 days of alpha glycerylphosphorylcholine on isometric strength. *Journal of the International Society of Sports Nutrition*, 12(1), 1–6.
56. Kolossa, D., Azhar, B., Rasche, C., Endler, S., Hanakam, F., Ferrauti, A., & Pfeiffer, M. (2017). Performance estimation using the fitness-fatigue model with Kalman filter feedback. *International Journal of Computer Science in Sport*, 16(2), 117–129.
57. Matabuena, M., & Rodríguez-López, R. (2019). An improved version of the classical banister model to predict changes in physical condition. *Bulletin of Mathematical Biology*, 81, 1867-1884.
58. Philippe, A. G., Borrani, F., Sanchez, A. M., Py, G., & Candau, R. (2019). Modelling performance and skeletal muscle adaptations with exponential growth functions during resistance training. *Journal of Sports Sciences*, 37(3), 254–261.
59. Imbach, F., Sutton-Charani, N., Montmain, J., Candau, R., & Perrey, S. (2022). The use of fitness-fatigue models for sport performance modelling: Conceptual issues and contributions from machine-learning. *Sports Medicine - Open*, 8(1), 29.



doi:10.6342/NTU202501357

# 個人期刊論文發表

此碩士論文之部分研究成果，已經以期刊論文的型式發表於學術期刊(共一篇)。以下是這篇期刊文的相關資訊：

期刊論文題目：Feasibility of Using Optimal Control Theory and Training-Performance Model to Design Optimal Training Programs for Athletes

作者：Yi Yang，Che-Yu Lin

發布日期：2025/6/30

期刊：CMES - Computer Modeling in Engineering & Sciences

冊別：143

期數：3

頁數：2767-2783

發布機構：Tech Science Press

論文網頁：https://www.techscience.com/CMES/v143n3/62812



doi:10.6342/NTU202501357